POLITECNICO DI TORINO

Master of Science in Aerospace Engineering

Academic Year 2023-2024
Master Thesis

Optimization of interplanetary transfers with flybys and deep-space maneuvers

Advisor:
Prof. Lorenzo CASALINO

TAS-I Tutors:
Dr. Giorgio FASANO
Ing. Andrea D'OTTAVIO

Candidate:
Giorgio PESENTI

April 2024

Acknowledgements

Ringrazio il Prof. Casalino per la revisione della tesi.
Ringrazio il Dr. Giorgio Fasano, guida fondamentale in questi mesi, per la grande disponibilità e i preziosissimi consigli e l'Ing. Andrea D'Ottavio per il supporto e per aver creduto fortemente nel lavoro svolto. Ringrazio inoltre tutti gli altri ragazzi dell'ufficio di Mission Analysis e Operations, sempre disponibili per fornire consigli e aiuto. Con la loro passione e simpatia hanno reso molto piacevoli i sei mesi passati in ufficio.
La tesi arriva, però, solo negli ultimi sei mesi di un percorso lungo quasi sei anni e ci sono alcune persone molto importanti nella mia vita a cui va la mia gratitudine.
Ringrazio Alessandro e Edoardo, i miei amici storici e inseparabili, con cui, nonostante la distanza, mantengo un rapporto per me fondamentale. Ringrazio Simone, conosciuto il primo giorno di Politecnico e sempre presente in questi anni, con le innumerevoli salite al Monte dei Cappuccini. Ringrazio Dario e Giacomo, nuovi amici, (quasi) sempre presenti alle serate ottimizzazione.
I ringraziamenti più sentiti vanno però alla mia famiglia, a mia sorella Martina, ai miei genitori Rossella e Sergio e ai miei nonni Rina e Gino. Il mio percorso di studi è stato possibile grazie a loro, perché con il loro supporto ho potuto concentrarmi sullo studio senza pensieri. Hanno accettato le mie scelte, hanno sempre avuto fiducia in me e, cosa più importante, mi vogliono un bene immenso.

A tutti voi, di nuovo, un ringraziamento sincero.

Cogoleto, Marzo 2023.
Giorgio.

Abstract

Interplanetary scientific missions pose several challenges for trajectory analysis because a direct transfer is often not possible due to the high delta-v. On the other hand, flybys and deep-space maneuvers allow a reduction of this delta-v at the cost of increased complexity in the trajectory. A well-known example of such an ambitious mission is the Cassini-Huygens robotic spacecraft.

The study here presented focuses on the optimization of high-thrust interplanetary transfers with multiple flybys and deep-space maneuvers. A direct optimization method including black boxes is used to minimize the total delta-v in the presence of mission constraints. The complexity of these trajectories poses several challenges to the optimization process, due to the overall non-convexity and the significant number of variables and constraints involved. As finding the global minimum represents a very challenging task, an optimization process consisting of several successive steps is developed. In the first optimization phase, the two-body-patched-conics model is used (See e.g., [1]). This allows to use a local optimizer (SQP) recursively to find many solutions in a reasonable time, in the perspective of obtaining the global optimum. For particularly complex problems, with longer flyby sequences and many constraints, an evolutionary algorithm is used at first to identify good guess solutions and to tighten the bounds of variables.

An ad-hoc heuristic approach has been developed for the second phase to explore alternative solutions more efficiently compared to a multipurpose "multi-start" algorithm, allowing to reduce the number of starting points. Eventually, the major results are presented to demonstrate the validity of this method in comparison with previous missions. Furthermore, a method has been developed to solve the Boundary Value Problem in the case of perturbed dynamics, with the aim of extending the approach to more detailed analyses in the future. The method, implemented in the Python environment, allows the addition of constraints with flexibility, guiding the user from problem definition to the optimal trajectory.

[1] M. R. Sentinella and L. Casalino. "Hybrid Evolutionary Algorithm for the Optimization of Interplanetary Trajectories". In: Journal of Spacecraft and Rockets 46.2 (2009), pp. 365–372.

Contents

List of Figures

List of Tables

Chapter 1

Introduction

Figure 1.1: The solar system.

Interplanetary missions provide valuable scientific insights and contribute to our understanding of the solar system and beyond (*Figure 1.1*). Here are some aspects of scientific interest associated with interplanetary missions:

- **Origin and evolution of the Solar System:** By studying different celestial bodies, scientists can piece together the timeline of events that led to the formation of our sun and its surrounding planets. Landing or orbiting missions allow for the detailed study of the surface geology and composition of celestial bodies. This information helps scientists understand the geological history and potential resources of these bodies.
- **Atmospheric composition and dynamics:** Probing the atmospheres of planets help scientists understand their composition, temperature, and dynamics. This information is crucial for understanding the atmospheric conditions both for scientific

purposes and for future landings.

- **Search for extraterrestrial life:** Interplanetary missions often aim to search for signs of life or conditions that might support life. This involves studying the presence of water, organic molecules, and other possible traces of past or present life.
- **Technological advancements:** The development of technologies for interplanetary missions often leads to advancements in space exploration and other fields. These innovations can have practical applications on Earth as well. An example could be the development of advanced technology for generating electric power from the sun or storing electrical energy.
- **Inspiration and Education:** Interplanetary missions capture the public's imagination and inspire the next generation of scientists and engineers. These missions often serve as educational tools and can foster a broader interest in science and space exploration.

Following the launch of Sputnik 1 in 1957 [1], both the United States and the Soviet Union began various interplanetary exploration programs.

The **Pioneer Program (1958-1960)** marked the commencement of humanity's journey beyond Earth's orbit. Pioneer 1's successful lunar orbit in 1958 paved the way for subsequent missions, including the iconic Pioneer 10 and 11, which provided valuable data about Jupiter and Saturn.

Progressing into the 1960s and 1970s, the **Venera Program (1961-1984)** by the Soviet Union led the exploration of Venus. The historic achievement of Venera 7 in 1970, successfully landing on Venus and transmitting data back to Earth, demonstrated humanity's ability to study the harsh conditions of other planets.

Simultaneously, NASA's **Mariner Program (1962-1973)** played a crucial role in exploring the inner planets. Mariner 9, in 1971, became the first spacecraft to orbit Mars, providing detailed images of the Martian surface and advancing our understanding of its geology.

The monumental **Apollo Program (1961-1972)** marked the late 1960s and early 1970s, with six crewed Moon landings between 1969 and 1972. Apollo 11's historic moment, as astronauts Neil Armstrong and Buzz Aldrin took humanity's first steps on the lunar surface, remains etched in history.

Venturing further into the cosmos, the **Voyager Program (1977)** launched in 1977 and conducted a grand tour of the outer planets. Voyager 1 and 2 provided unprecedented insights into the outer planets and their moons, expanding our understanding of the solar system. Voyager 1 is also the first human-made object to venture into interstellar space.

As the 1980s dawned, **Magellan (1989-1994)** focused on Venus, utilizing radar mapping to unveil the planet's topography and geology. The mission significantly enhanced our knowledge of Venusian features, including volcanoes and impact craters.

The**Mars Pathfinder (1996)** mission successfully landed the Sojourner rover on Mars, marking the first steps in exploring the Martian surface and conducting on-site analysis of rocks and soil.

The joint **Cassini-Huygens (1997)** (*Figure 1.2*) mission supported by NASA, ESA, and ASI provided a comprehensive exploration of Saturn and its moon Titan. Cassini's

extensive data collection included studies of Saturn's rings, atmosphere, and moons, while the Huygens probe's descent onto Titan in 2005 marked a historic landing.

Figure 1.2: An artistic illustration of the Cassini probe before its final dive into Saturn's atmosphere.

The **Mars Exploration Rovers (2003)**, Spirit and Opportunity, undertook extensive exploration of the Martian surface, studying rocks and soil for signs of past water activity. These resilient rovers exceeded their planned mission durations, contributing significantly to our understanding of Mars.

ESA's Rosetta (2004): Rosetta, a mission led by the European Space Agency, achieved historic milestones by orbiting and deploying the Philae lander to Comet 67P/Churyumov-Gerasimenko in 2014. The spacecraft conducted detailed studies of the comet's nucleus and its interactions with the solar wind. The mission concluded in 2016 when Rosetta descended onto the comet's surface, providing unprecedented data on cometary composition.

In the mid-2000s, **New Horizons (2006)** embarked on a historic flyby of Pluto and the Kuiper Belt, providing the first close-up images of this distant dwarf planet and advancing our knowledge of the outer solar system.

The **Mars Science Laboratory (Curiosity) (2011)** landed the Curiosity rover on Mars in 2012, initiating a mission focused on studying the planet's past habitability and potential for microbial life. In 2011, the **Juno (2011)** spacecraft entered orbit around Jupiter, commencing a mission that aimed to study the giant planet's composition, gravity field, and magnetosphere, shedding light on its formation and evolution.

OSIRIS-REx (2016) (Origins, Spectral Interpretation, Resource Identification, Security, Regolith Explorer) successfully reached the near-Earth asteroid Bennu in 2018. The spacecraft meticulously studied Bennu's surface and, in 2020, collected a sample of regolith, or asteroid soil. It returned to Earth on Sept. 24, 2023, to drop off material from asteroid Bennu. The spacecraft didn't land, but continued on to a new mission, OSIRIS-APEX, to explore asteroid Apophis.

The **Perseverance (Mars 2020)** rover, which landed on Mars in 2021, represents a significant step in exploring the Red Planet, with a focus on searching for signs of past microbial life and collecting samples for future return to Earth.

Ongoing efforts, such as NASA's **Artemis Program (2017)**, aim to return humans to the Moon by the mid-2020s, setting the stage for future crewed missions to Mars and further advancing human exploration of the solar system.

In the coming years, the European Space Agency (ESA) is getting ready for the **EnVision** mission, set for the early 2030s. This big mission aims to explore Venus thoroughly, checking out its surface, atmosphere, and geological features. The goal is to understand why Venus, a planet that seems similar to Earth in size and composition, is so different now.

Looking ahead in the 21st century, many upcoming missions are on the horizon, pushing humanity's quest for knowledge and exploration. One standout is the **Europa Clipper** mission, focusing on Jupiter's moon Europa. It plans to study the icy moon's surface and subsurface to see if it could support life in its large subsurface ocean.

There's also an exciting collaboration between NASA and the European Space Agency for the **Mars Sample Return** mission. This bold project aims to collect and bring back samples from the Martian surface, helping us learn more about Mars' geological history and the potential for past life.

These future missions are important steps in human exploration, promising to uncover the remaining mysteries of our solar system and beyond. The pursuit of knowledge and exploration of celestial bodies keeps pushing scientific efforts, revealing new frontiers and expanding our understanding of the vast cosmic landscape around us.

Interplanetary exploration faces challenges such as long communication delays, harsh environmental conditions, budget constraints, and overall high complexity. Additionally, limited payload capacity, precision navigation for accurate trajectories, challenges in entry, descent, and landing, and the necessity to launch within specific windows due to planetary alignment add complexity to mission planning and execution. As for aspects related to trajectory analysis, the critical aspects are:

- **Limited Payload Capacity:** Launch vehicles have limited payload capacities, making it challenging to send large and heavy payloads on interplanetary missions. This limitation affects the size and capabilities of scientific instruments, rovers, and other equipment that can be included in a spacecraft.

- **Precision Navigation:** Navigating through interplanetary space requires precise calculations and adjustments. Small errors in navigation over long distances can lead to significant deviations from the intended trajectory. Mission planners need to account for gravitational influences and other sources of perturbation to ensure spacecraft reach their destinations accurately.

- **Entry, Descent, and Landing (EDL):** Safely landing on a planetary surface presents unique challenges. The thin atmospheres of some planets make traditional landing techniques challenging. Developing technologies for precise EDL, especially for larger payloads like rovers, is a critical aspect of mission planning.

- **Limited Launch Windows:** Interplanetary missions must be launched during specific windows when the planets are properly aligned. These launch windows are often narrow and may occur only once every couple of years, requiring precise mission planning and scheduling.

Given these difficulties, the optimization of interplanetary trajectories plays a crucial role from the early stages of the mission and is often enabling for the mission itself.

A typical interplanetary scientific mission can be divided into several phases:

- **Launch**: The launch phase marks the initial stage of the mission. The launch vehicle imparts the probe with the required DeltaV to either place it into a parking orbit or, in the case of a direct escape, directly into Earth's escape orbit. This phase aims to meet the conditions necessary for the spacecraft to escape Earth and embark on its interplanetary journey.

- **Interplanetary Transfer**: In this phase, the spacecraft moves along the trajectory that will take it from the departure planet to the targeted celestial body. Flybys and Deep-Space Maneuvers (DSMs) may occur during this phase. DSM refers to deterministic maneuvers that do not occur in the vicinity of celestial bodies. From a mission analysis perspective, this phase is crucial because the feasibility of the mission depends on it.

- **Capture**: The capture phase entails a series of maneuvers necessary to shift the spacecraft from a hyperbolic arrival orbit to the science orbit. This can be achieved through thruster burns or by utilizing the atmosphere of the target body, if present. In this case, it is referred to as aerobraking or aerocapture depending on the particular technique.

- **Science Phase**: The science phase is when the probe accomplishes its scientific objectives. The orbit during the science phase is typically a constraint for interplanetary transfer, as the altitude and inclination of this orbit must allow the achievement of scientific goals.

Optimization plays a critical role in maximizing payload mass (or, conversely, minimizing propellant mass). Trajectories often become intricate due to the prohibitively high cost of a direct Hohmann-like transfer. Consequently, trajectories frequently incorporate flybys, allowing for the alteration of the spacecraft's path with minimal or significantly limited use of propellant.

An example of this type of trajectory is that of the Cassini-Huygens probe in *Figure 1.3*.

The complexity of the problem demands special attention to the optimization process and the utilization of techniques that enable achieving a global optimum even in the presence of multiple constraints and a large number of variables.

This thesis focuses on the examination and optimization of interplanetary transfers, considering constraints on the final orbit, launch limitations, and additional factors such as maximum duration.

The primary goal of this thesis is to develop an optimization tool for the preliminary analysis of such missions.

Preliminary analysis refers to an examination approach designed to assess various solutions within reasonable time to select one or more baselines. In this phase, simple dynamic models are employed to facilitate efficient optimization.

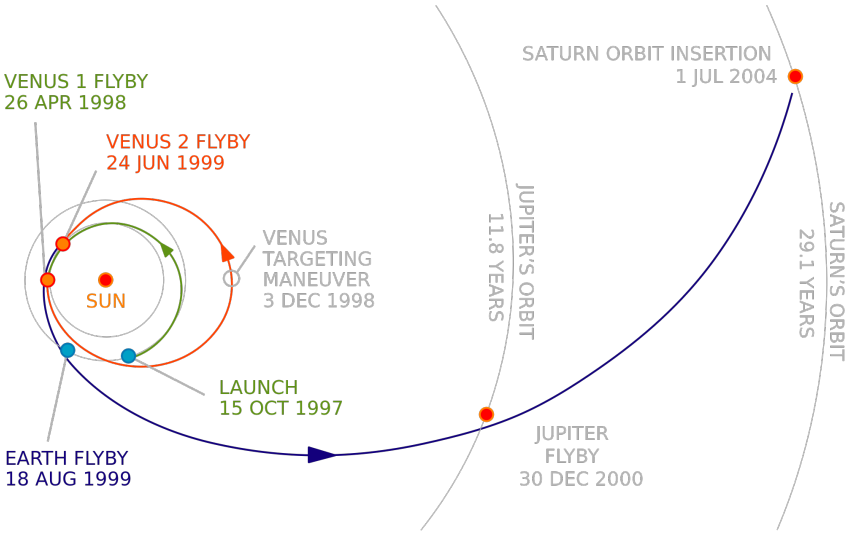

Figure 1.3: Interplanetary trajectory of the Cassini-Huygens probe.

As a secondary objective, various techniques have been developed with the goal of extending the method in the future to a more detailed analysis, considering dynamics with perturbations.

To achieve this goal, these actions have been undertaken:

- Formulation as an optimization problem.
- Development of a set of strategies to solve the optimization problem in the presence of constraints to achieve global optimum.
- The method has been implemented into a tool that facilitates the formulation and resolution of problems. This tool guides users through defining a scenario, comprising a sequence of celestial bodies and a launch window, and allows for the specification of constraints. It then efficiently solves the problem and presents the results.
- Application of the method to various scenarios, including some past missions used as benchmarks to verify the ability to identify a global optimum.
- Extension of the method to more complex cases where complete dynamics are considered.

The thesis comprises six chapters that cover various aspects of the research. The second chapter focuses on optimization and discusses the strategies employed in detail. Chapter three provides an overview of the method and the physical models used. The fourth chapter presents the main results achieved, including benchmarks with past missions. Chapter five outlines the steps taken to extend the method for more detailed analysis involving perturbations. Finally, chapter six contains the conclusions.

Chapter 2

Optimization

This thesis deals with complex optimization problems which are non-convex and require global optimization strategies. This chapter will discuss general aspects of optimization. It starts with a brief introduction about the optimization problems and the different strategies used today. It proceeds to present some concepts about black-box optimization and finally, the strategies and methods adopted are presented in detail.

2.1 Introduction to optimization

Optimization is a systematic approach aimed at discovering the optimal solution, typically the maximum or minimum, for a given mathematical model or function while adhering to specified constraints. The objective is to pinpoint the most favorable values for variables that result in optimal outcomes, be it maximizing profit, minimizing costs, optimizing efficiency, or achieving any other desired goal.

Optimization problems are commonly classified based on their main characteristics.

Dimensionality Problems can be finite-dimensional or infinite-dimensional. In the former, a finite number of real or integer decision variables are involved, while in the latter, decision variables are functions.

Convexity Convexity and non-convexity are crucial properties in optimization problems, significantly impacting solvability. Convex problems are notably easier to solve due to the absence of local minima and the convergence of local search algorithms to the global optimum (*Figure 2.1*).

Number of objectives Optimization problems can be classified based on the number of objectives. Single-objective optimization involves the minimization of a single objective function, while multi-objective optimization deals with conflicting objectives that need simultaneous optimization. Instead of a single optimal solution, multi-objective optimization seeks a set of solutions known as the Pareto front. A solution is considered Pareto optimal if no other solution in the search space improves one objective without degrading at least one other objective.

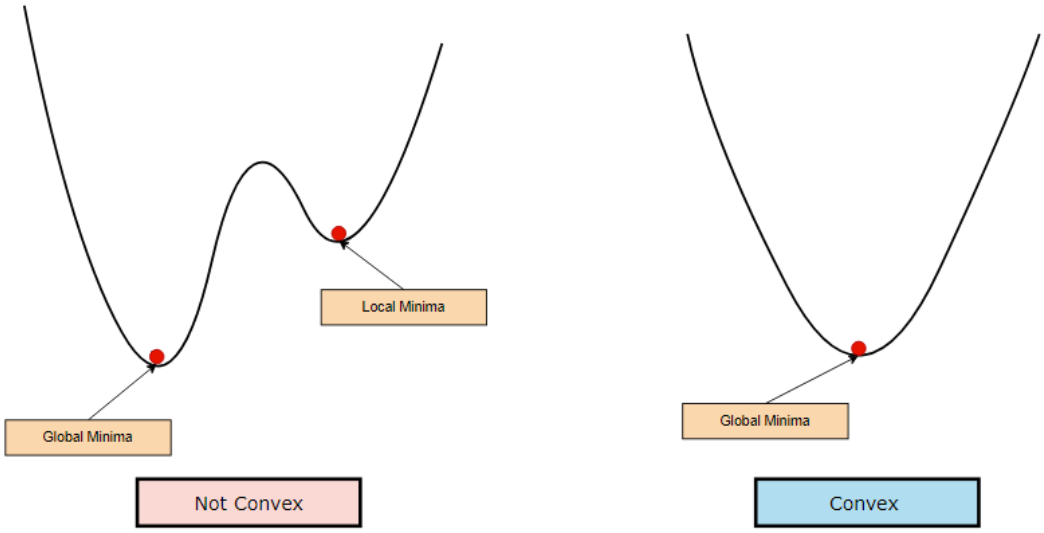

Figure 2.1: Examples of convex and non-convex functions.

Form of the cost function and the constraints The structure of the cost function and constraints is another important feature. The main categories include Linear Programming (LP), where both the objective function and the constraints are linear, and Nonlinear Programming (NLP), where either the objective function or the constraints (or both) involve a non-linear relationship. An important sub-category is Quadratic Programming (QP), dealing with a quadratic objective function and linear or quadratic constraints.

Type of variables Another distinction can be made based on the type of variables. Typically, the variables are real values, but in some cases, all variables (Integer Programming, IP) or some variables (Mixed Integer Programming, MIP) must be integers.

There are various optimization problems, and selecting the most appropriate strategies based on the specific problem is essential.

2.1.1 Problem statement - Optimal control problem

An optimal control problem is a mathematical framework that deals with the optimal management of dynamic systems. In this context, a dynamic system refers to a set of interrelated variables or states that evolve over time, influenced by control inputs or actions. The objective of optimal control is to find a control policy – a set of rules or strategies for manipulating the system – such that a certain performance criterion is optimized.

The performance criterion is expressed as an objective function that quantifies the desirability of system behavior. This could involve maximizing or minimizing a certain outcome, taking into account the effects of control inputs, system dynamics, and external disturbances. The optimal control problem typically considers constraints on the system states, control inputs, and other relevant variables.

The solution to an optimal control problem involves determining the optimal trajectory of control inputs over time, considering the system dynamics and constraints, to achieve the best possible performance according to the specified criterion.

A common formalism is the *Bolza formulation* (See e.g. [2]). The function to be minimized (or equivalently maximized) is called *objective function* J_B.

$$J_B = \varphi(\boldsymbol{x}_{(j-1)_+}, \boldsymbol{x}_{j_-}, t_{(j-1)_+}, t_{j_-}) + \sum_j \int_{t_{(j-1)_+}}^{t_{j_-}} \phi\left[\boldsymbol{x}(t), \boldsymbol{u}(t), t\right] dt, \quad j = 1, ..., p$$

where:

- $\boldsymbol{x}(t)$ is the state variable vector,
- $\boldsymbol{u}(t)$ is the control variable vector,
- t is the independent variable.

$(x_{0_+}, x_{1_-}), ..., (x_{(n-1)_+}, x_{p_-})$ are the trajectory arcs.

The state variables are subject to the state equations, where the system dynamics are modeled:

$$\dot{\boldsymbol{x}}(t) = \boldsymbol{f}\left[(\boldsymbol{x}(t), \boldsymbol{u}(t), t)\right]$$

The system is also subject to *boundary conditions*:

$$\chi(\boldsymbol{x}_{(j-1)_+}, \boldsymbol{x}_{j_-}, t_{(j-1)_+}, t_{j_-}), \quad j = 1, ..., p$$

and additional *constraints*:

$$\boldsymbol{g}\left[(\boldsymbol{x}(t), \boldsymbol{u}(t), t\right] \leq 0$$

2.1.2 Common optimization methods

Various approaches are employed to address optimization problems, and a common classification is outlined below.

Direct methods These techniques utilize discretization to convert the optimal control problem into a finite-dimensional optimization problem (NLP) and directly solve it.

Indirect methods This category relies on necessary (and sufficient) conditions for optimality, such as Pontryagin's maximum principle, to tackle the optimal control problem in the form of a boundary value problem (BVP).

Evolutionary algorithms These methods harness large populations of solutions that evolve according to specific rules, aiming to converge towards the global optimum.

Others Simulation approaches, like single/multiple shooting, prove beneficial for simple problems or situations where highly accurate initial solutions are available.

2.1.3 Black box optimization

Black-box optimization becomes essential when the structure of the cost function and/or constraints is unknown, commonly encountered when dealing with non-convex cost functions and unknown gradients.

The overarching framework of black-box optimization, illustrated in *Figure 2.2*, comprises a *simulation part* and an *optimization part*. In the simulation phase, the cost function and constraints are assessed for a set of data, encapsulating the problem within a black box. The output from this black box becomes the input for the optimization part, where an algorithm iteratively computes a new value for $\boldsymbol{u}$. This cycle repeats until certain conditions are met, ideally leading to a satisfactory solution.

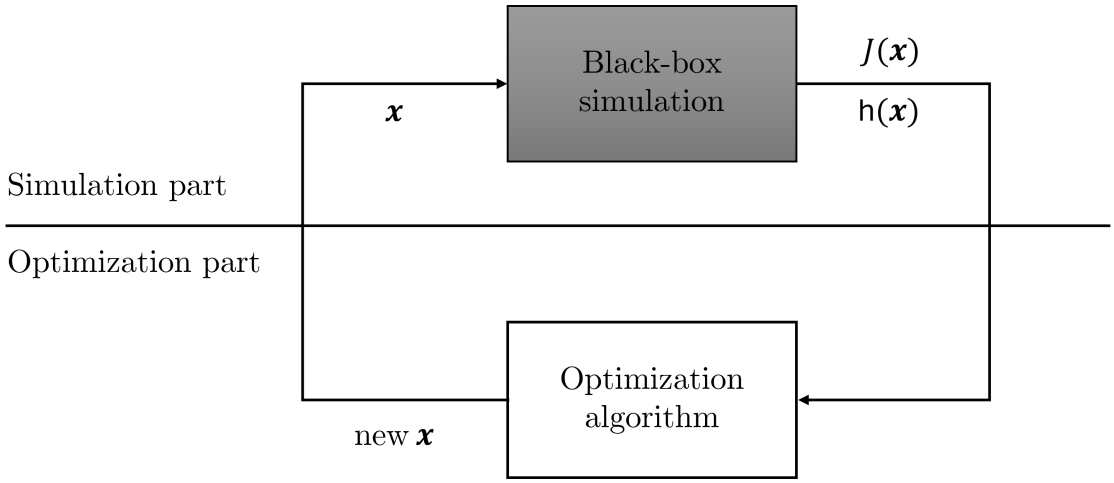

Figure 2.2: Black-box optimization.

Using a black-box approach allows formulating the problem with a reduced number of input variables. For instance, in the context of a high-thrust trajectory, breaking down the trajectory into a specific number of ballistic arcs allows for a simpler parameterization. In this scenario, the initial conditions and the duration of each segment could form a set of variables for the black box.

An alternative method could be the direct collocation approach. The direct collocation method is a numerical approach for solving optimal control problems with continuous dynamics. The process begins by discretizing the time interval into a finite number of nodes. Subsequently, both state and control variables are discretized at these nodes, transforming the continuous functions into vectors or arrays. The differential equations describing the system dynamics are then approximated at these nodes using finite differences, resulting in a set of algebraic equations. The key feature of direct collocation is the enforcement of system dynamics not only at the endpoints but also at intermediate points through collocation constraints, ensuring that the approximated dynamics adhere closely to the original differential equations.

Using this method significantly increases the number of variables since it requires discretizing the trajectory into shorter intervals, amplifying the complexity of the optimization problem.

2.2 A focus on the adopted optimization methods

This section explains the optimization algorithms utilized in this thesis. The objective of the thesis is to create a versatile tool applicable to various scenarios, capable of identifying the global solution or, at the very least, a highly effective one. Strict adherence to certain constraints was necessary, while others allowed for greater tolerances.

Existing literature, as indicated by Vasile [3] and Ceriotti [4], emphasized the pronounced non-convex nature of the problem. Initial tests revealed that a conventional local search, like Multistart from random points, succeeded only in simpler cases involving a limited flyby sequence of 3-4 bodies.

To achieve a universally applicable tool, a hybrid method was adopted. This method combines an evolutionary algorithm, ad-hoc heuristic, and a conventional multistart with Sequential Quadratic Programming (SQP).

The primary objective was to devise a strategy capable of uncovering the global optimum in diverse scenarios involving various body sequences and constraints. It's important to note that time efficiency was not the primary concern, as this trajectory optimization occurs on the ground.

2.2.1 Evolutionary algorithms

Evolutionary algorithms (EAs) are optimization algorithms inspired by the process of natural selection. They are used to find solutions to optimization and search problems by mimicking the principles of biological evolution. Many evolutionary algorithms have been developed over the years. They all share all (or some) of the steps reported above but each algorithm is characterized by specific methods and criteria for selection, crossover, mutation, and replacement.

A non-exhaustive list of evolutionary algorithms is reported.

- **Genetic Algorithms (GAs):** Crossover and mutation operators are applied to the population members.
- **Differential Evolution (DE):** It generates trial solutions through the combination of differences between randomly selected individuals in the population.
- **Particle Swarm Optimization (PSO):** Inspired by the social behavior of birds and fish. It uses a population of particles that move through the search space, adjusting their positions based on their own best-known position and the swarm's best-known position.
- **Ant Colony Optimization (ACO):** Inspired by the foraging behavior of ants. It involves constructing solutions by simulating the paths of ants in search of food.

Evolutionary algorithms consist of several steps.

1. **Initialization:** A population of potential solutions is generated. The initial population can be chosen randomly or based on guess solutions.

2. **Evaluation:** The cost function of each solution in the population is computed and the constraints violation is typically added with a penalty weight to the cost function. The value of this cost function with penalties is typically referred to as *fitness*.

3. **Selection:** Solutions are selected for reproduction based on their fitness. Solutions with higher fitness are more likely to be selected for the next generation.

4. **Crossover:** Pairs of selected solutions exchange genetic information to produce new solutions. This mimics the recombination of genetic material in biological evolution.

5. **Mutation:** Random changes are introduced to some of the solutions in the population. This introduces diversity and helps explore the search space.

6. **Replacement:** The new offspring and some of the existing solutions make up the next generation. The least fit solutions may be replaced by the offspring, maintaining the population size.

7. **Termination:** The process is repeated for a predefined number of generations or until a termination criterion is met (e.g., convergence to a satisfactory solution).

Differential Evolution

Differential Evolution (DE) is a simple yet powerful evolutionary algorithm (EA) for global optimization introduced by Price and Storn [5]. The population can be initialized randomly or from a set of guess solutions. If the number of available guess solutions is lower than the individual number n, the remaining individuals are generated randomly between the variables' boundaries or perturbing the existent solutions.

DE generates new vectors of variables by adding the weighted difference between two population vectors to a third one according to this *mutation* scheme:

$$\text{Mutant Vector[i]} = \text{Target Vector[a]} + F(\text{Target Vector[b]} - \text{Target Vector[c]})$$

$$i = 1,2,...,n \qquad a, b, c \in [1 : n]$$

where F is a real number that controls the amplification of the difference vector. If a component of a mutant vector goes off the box, then this component is set to a bound value. This basic principle can be varied and there are several practical variants of DE. For example, a linear combination of two vectors, instead of three, can be used to determine the new individuals or a comparison can be made between the new vector and the best individual, instead of one chosen randomly.

The target vector is mixed with the mutated vector using the following *crossover* scheme, to yield the *trial vector*:

$$\text{Trial vector}[i][j] = \begin{cases} \text{Mutant vector}[i][j] & \text{if r(j)} \leq CR \text{ or } j = \text{rand(i)} \\ \text{Current vector}[i][j] & \text{otherwise} \end{cases}$$

$$i = 1,2,...,NP \quad j = 1,2,...,D$$

where D is the number of components of the variables vector. It's important to note that the crossover operation is applied element-wise, allowing for a diverse combination of

genetic material from both the mutant and current vectors. This element-wise approach helps maintain diversity in the population, aiding the algorithm in escaping local minima and converging to a global optimum.

If the resulting individual exhibits a higher fitness than a predetermined population member, in the next generation the new individual replaces the one it was compared with; otherwise, the old individual is retained.

Evaluate the trial vectors using the objective function and select vectors that outperform their corresponding base vectors to form the next generation:

$$\text{Next generation}[i] = \begin{cases} \text{Trial vector}[i] & \text{if } f(\text{Trial vector}) < f(\text{Current vector}) \\ \text{Current vector}[i] & \text{otherwise} \end{cases}$$

where f is the objective function.

Self-Adaptive Differential Evolution In the classic DE algorithms, both the F and the CR parameters must be tuned by the user. Adequate tuning is very important for algorithm convergence and can be problem-dependent.

To develop an easy-to-use tool, an interesting evolution of DE, called Self-Adaptive Differential Evolution (SADE) offers a valuable alternative. In [6] a self-adaptive approach for control parameters is presented. The control parameters are calculated as:

$$\text{Next generation } F[i] = \begin{cases} F_l + rand_1 * F_u & \text{if } rand_2 < \tau_1 \\ F[i] & \text{otherwise} \end{cases}$$

$$\text{Next generation } CR[i] = \begin{cases} rand_3 & \text{if } rand_4 < \tau_2 \\ CR[i] & \text{otherwise} \end{cases}$$

The additional parameters are constant:

$$F_l = 0.1,\ F_u = 0.9 \quad \tau_1 = \tau_2 = 0.1$$

The inclusion of an extra evolutionary process known as *mass mutation* as explained in [7], is under consideration. Should the dominant individual within the population persist without change for a specified number of generations, a designated percentage of individuals is retained, while the rest undergo random re-initialization. This approach proves beneficial in guarding against premature convergence to local minima. Although these parameters necessitate careful calibration, a recommended benchmark includes $\eta = 0.35$(the retention percentage) and $GEN_{mm} = 50$ (the interval between opportunities for mass mutation).

SADE does not need the user to provide good values for F and CR offering the advantage of being less problem-specific. DE with *good* parameter choice could perform better than SADE but requires several tuning runs.

SADE proved to be effective in solving the optimization problems of this thesis and therefore was chosen as the first step of the global optimization strategy.

2.2.2 Multistart + SQP

Multistart combined with Sequential Quadratic Programming (SQP) is an optimization strategy employed to discover the global minimum of a nonlinear and nonconvex objective function, leveraging the capabilities of a local optimization method.

The nonconvex nature of the function necessitates a *global* strategy since relying solely on a local search algorithm proves insufficient for uncovering the global optimum.

Multistart, a global optimization technique, entails running a local optimization algorithm multiple times from diverse initial points in the search space. This approach aims to explore a wider region of the solution space, thereby enhancing the probability of identifying a global minimum.

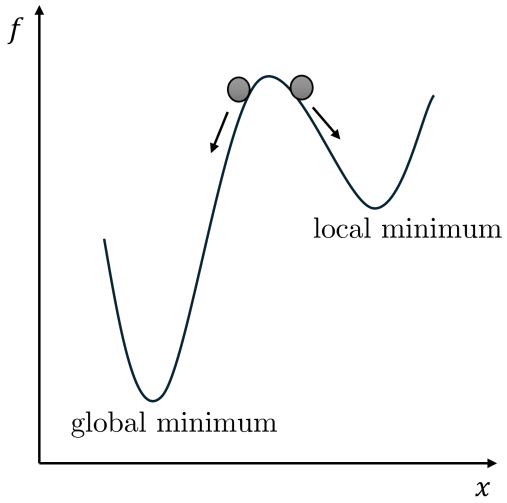

Figure 2.3: Local minimization from different starting points.

SQP is a local optimization method used for solving nonlinear-constrained optimization problems. The algorithm makes use of a local quadratic approximation to model the nonlinear objective function and constraints.

After running SQP from a high number of starting points, the best solution found among all runs is considered the potential global minimum.

The advantage of the combination of Multistart and SQP lies in its simplicity but the random choice of the starting point can be insufficient to solve difficult problems.

2.2.3 Ad-hoc heuristic for global optimization

An *ad-hoc* heuristic has been devised to navigate the solution space starting from a known solution. The approach involves maximizing the *Euclidean distance* of a variable vector from the current solution while maintaining the cost function value below a specified threshold. This heuristic proves beneficial for exploring alternative minima, providing improved starting points for local searches compared to the random approach of a typical Multistart algorithm.

The optimization problem is initially defined as follows:

$$\text{Optimization problem: } \begin{cases} \text{Cost function: min } J(\boldsymbol{x}) \\ \text{Constraints : } h(\boldsymbol{x}) \leq 0 \end{cases} \rightarrow J^*(\boldsymbol{x}^*),\ \boldsymbol{x}^*$$

A modified optimization problem is formulated by maximizing the Euclidean distance while still adhering to constraints and maintaining the cost function below the original minimum plus a margin:

$$\text{Modified problem: } \begin{cases} \text{Cost function: max } \|\boldsymbol{x} - \boldsymbol{x}^*\| \\ \text{Constraints : } h(\boldsymbol{x}) \leq 0 \text{ and } J(\boldsymbol{x}) \leq kJ^*(\boldsymbol{x}^*) \end{cases} \rightarrow \boldsymbol{x}^{**}$$

The parameter k allows solutions to exceed the original cost function value, essential for escaping local minima (*Figure 2.4*. The resulting $\boldsymbol{x}$ is then utilized as a starting point for a new local search. This heuristic strategy can be generalized by introducing a *weight vector*

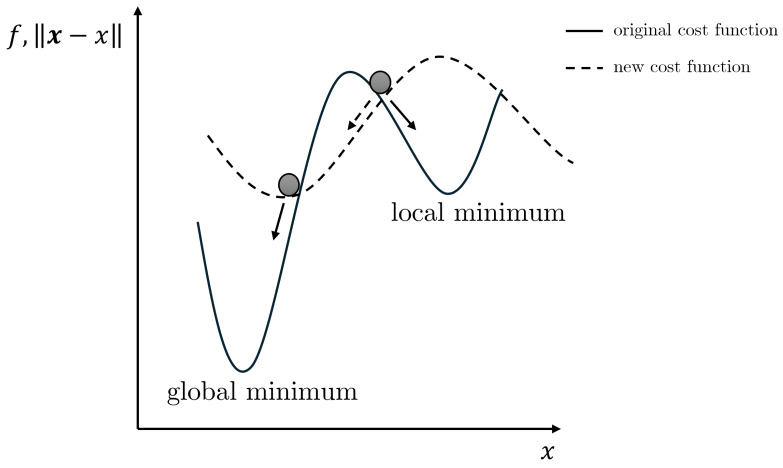

Figure 2.4: Ad-hoc heuristic.

to the vector difference, allowing movement in different directions:

$$\text{Modified problem: } \begin{cases} \text{Cost function: max } \|\boldsymbol{w}(\boldsymbol{x} - \boldsymbol{x}^*)\| \\ \text{Constraints : } h(\boldsymbol{x}) \leq 0 \text{ and } J(\boldsymbol{x}) \leq kJ^*(\boldsymbol{x}^*) \end{cases} \rightarrow \boldsymbol{x}^{**}$$

The weight vector can be employed to *force* diversification along certain components, useful for generating a set of new starting points for local searches or initializing a population for an evolutionary algorithm.

Two main advantages of this method are:

- Feasibility of the new starting points.
- Proximity of the original cost function value for the new starting points to the known optimum.

Another approach to generating additional starting points involves considering a specified number of points between the known minimum and the solution to the modified

optimization problem. This method can be regarded as a path-relinking technique, where two existing solutions are recombined to explore the solution space in order to achieve an improved solution. [8]

This is achieved through component-wise interpolation (*Figure 2.5*):

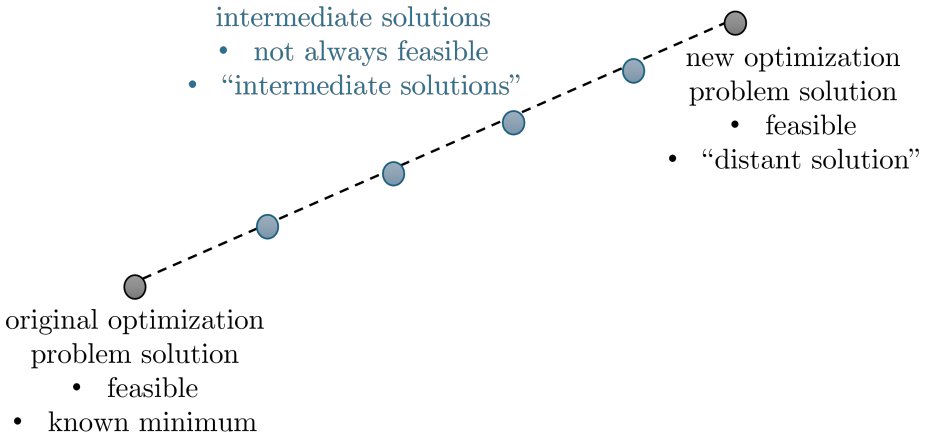

Figure 2.5: Intermediate solutions.

In this general method, the user must choose three parameters. The k parameter governs the movement toward a worse solution, influencing the algorithm's freedom to explore the solution space.

The weight vector $\boldsymbol{w}$ can be varied to enhance diversification along specific components, either randomly or purposefully. For instance, in a problem where a specific delta-v is given at a given instant, the user might want to explore solutions by keeping the delta-v fixed but varying the date.

The number of intermediate points can be chosen arbitrarily, as they are obtained through simple linear interpolation.

2.2.4 Global optimization strategies

The discussed algorithms are part of two overall optimization strategies. It's important to clarify that the goal here is not to find a single best method for the test problems, as achieving a universal approach in optimization is impractical. Rather, the focus has been on developing a versatile set of tools to handle these specific problems effectively. These strategies are detailed in the following sections and briefly summarized in the *Figure 2.6*.

The number of constraints in the problems may vary, typically limited to 3-4 inequality constraints. A conventional Multistart technique coupled with an SQP local solver has proven effective and efficient in discovering the global optimum when the body sequence is four or fewer. However, for longer sequences, such as in the Cassini test case, this approach falls short of finding the global optimum.

To address this limitation, a SADE algorithm is introduced as the initial optimization stage. Its primary purpose is to find at least a *good solution*, serving as a preliminary guess

solution for the subsequent stage. Additionally, this initial step aids in pruning the search space, significantly enhancing the subsequent Multistart + SQP method.

In the second optimization stage, both the classical Multistart + SQP and the ad-hoc developed heuristic + SQP are employed to obtain the global optimum. This stage serves as a refinement of the good solution obtained with the SADE algorithm, ensuring full adherence to all constraints.

The choice between the Multistart + SQP method and the ad-hoc heuristic depends on the problem's complexity. The Multistart + SQP method alone may suffice, but the ad hoc heuristic can enhance the efficiency of solution space exploration. Alternatively, this heuristic can be utilized to investigate different solutions that may not be the global minimum for the original cost function but possess interesting characteristics. This decision is problem-specific, requiring a case-by-case analysis by the user.

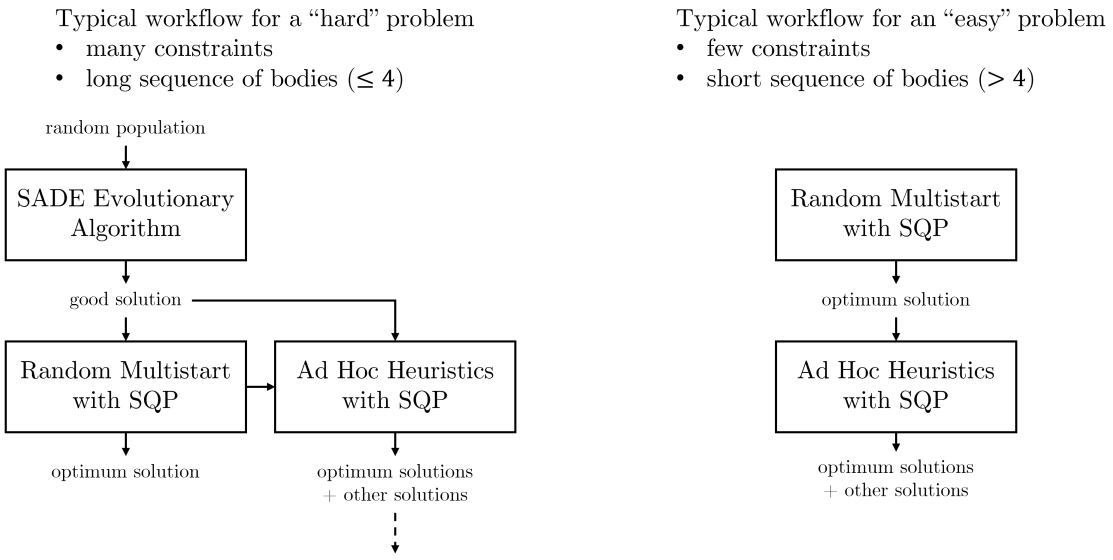

Figure 2.6: Global optimization strategies.

Chapter 3

Models

In this chapter, the general problem of interplanetary travel is first explained, followed by a detailed examination of the physical modeling aspects of interplanetary trajectory, launch phase, maneuver capture, and flybys.

3.1 Interplanetary transfer problem

The focus of this thesis involves the optimization of the delta-v required to reach a specific celestial body from Earth. A predetermined sequence of flybys is taken into consideration, with the option to execute deep-space maneuvers during various interplanetary segments, aiming to enhance the efficiency of space travel.

For the launch, a specific launch window $[\underline{t_0}, \overline{t_0}]$ is considered. In the preliminary analysis phases, different launch windows can be contemplated. For instance, if a mission can be launched within a certain period (e.g., between 2030 and 2035), this timeframe can initially be divided into sub-periods of 6 or 12 months to simplify the analysis. In subsequent phases, as initial solutions become available, launch windows are refined to the periods of interest.

The sequence of bodies $[B_0, B_1, \ldots B_n]$ represents an ordered series of celestial bodies, including the departure body, a series of intermediate bodies for flybys, and an arrival body. For complex missions to outer solar system celestial bodies, multiple flybys may be incorporated. The term "resonant flybys" is used when consecutive flybys occur around a planet.

In this work, the sequence is fixed a priori, but this does not preclude the possibility of exploring different combinations.

3.2 General problem formulation

The problem formulation utilizes a frequently employed model for preliminary analyses, often referred to as the Zero-Sphere-Of-Influence (ZSOI) patched conics (see e.g., [7]).

The name comes from the fundamental assumptions of the model. The spheres of influence of individual planets are considered negligible in size compared to heliocentric distances. The sphere of influence of a central body indicates a region in space where the

motion of the spacecraft is influenced more by the gravity of that object than by any other perturbation. For instance, the Earth's sphere of influence identifies the region of space where Earth's gravitational attraction dominates over that of the Sun and other planets.

A commonly used formula to estimate the radius of this sphere is as follows:

$$r_{SOI} = \left(\frac{m_\oplus}{m_\odot}\right)^{2/5} a_\oplus$$

where $m_\oplus$ and $m_\odot$ are respectively the mass of the planet (e.g. Earth) and the mass of the Sun, and $a_\oplus$ is the semimajor axis of the orbit of the Earth around the Sun.

For Earth, a radius of approximately 925,000 km is obtained, while the average Earth-Sun distance is 1 AU = 149,598,000 km. Their ratio is 0.006, making the assumption valid for preliminary analysis.

The second assumption is to divide the complete interplanetary trajectory into distinct segments that connect various planets, treating them as massless point objects. Each interplanetary segment between two planets is purely ballistic: the body moves along a Keplerian trajectory under the influence of the sun, with no perturbations or control actions present.

During this phase, departure, arrival, and flybys are considered instantaneous and point events, altering the spacecraft's state. These planetocentric phases are modeled separately, focusing only on what occurs within the sphere of influence of the respective bodies. Once again, a Keplerian motion is assumed, where the only gravitational force is that of the central body.

This simplification allows for the "decoupling" of the interplanetary transfer problem (heliocentric phase) from the various planetocentric phases, giving rise to the term "patched-conics."

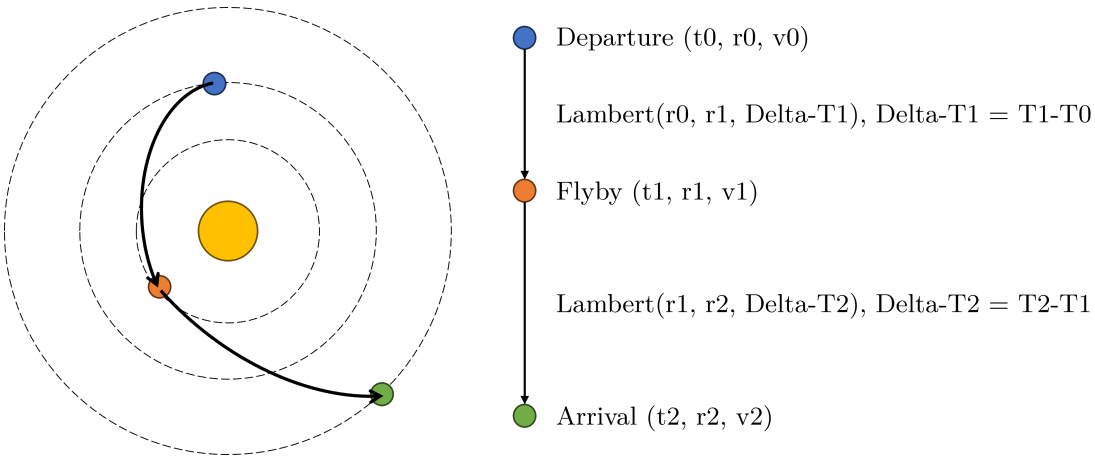

Figure 3.1: An interplanetary transfer with an intermediate flyby.

The diagram in Figure 3.1 illustrates an interplanetary transfer between two planets, including an intermediate flyby. The aforementioned assumptions allow the formulation of the various segments as Lambert's problems. Lambert's problem involves determining the orbit when provided with an initial point, a final point, and the flight time between the

two points. This is done under the assumptions of the restricted two-body problem. The term takes its name from the Swiss mathematician Johann Heinrich Lambert, who first formulated it in the 18th century.

The solution to Lambert's problem allows obtaining the velocity at the initial and final points. By solving the different segments of Lambert, it is possible to obtain the velocities in the heliocentric system at the beginning and end of each segment. These points correspond to the center of mass of the various bodies in the sequence.

The position and velocity of each planet can be calculated using ephemerides, which are tables containing pre-calculated values for a specific time interval.

To evaluate the various planetocentric phases, it is necessary to know the asymptotic velocity V_∞.

The asymptotic velocity refers to the velocity of an object in space as it approaches an infinite distance from any gravitational source.

$$\frac{V_\infty^2}{2} - \frac{\mu}{r} = -\frac{\mu}{2a}$$

$$V_\infty = \sqrt{\frac{2\mu}{r} - \frac{\mu}{a}}$$

$$V_\infty = \sqrt{\frac{2\cancel{\mu}}{\cancel{r}} - \frac{\mu}{a}} = \sqrt{-\frac{\mu}{a}} \tag{3.1}$$

In this simplified model, V_∞ can be expressed as the relative velocity of the spacecraft with respect to the planet (*Figure 3.2*).

$$V_\infty = V_{S/C} - V_P$$

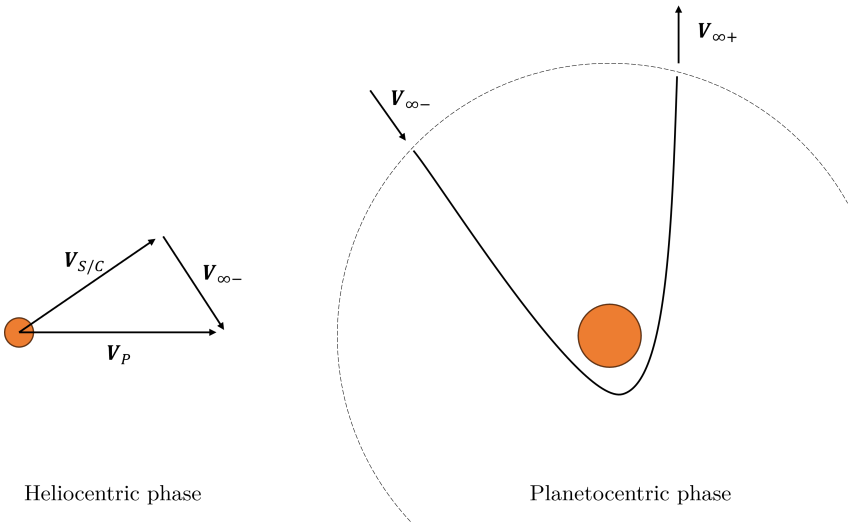

Figure 3.2: Heliocentric and planetocentric phase.

The possibility of performing a Deep Space Maneuver (DSM) during interplanetary segments can be included by dividing the transfer between two planets into two separate segments. (*Figure 3.3*) This additional degree of freedom for the trajectory can offer benefits in terms of reducing the overall DeltaV, especially in synergy with gravity assists, to achieve more favorable flyby conditions.

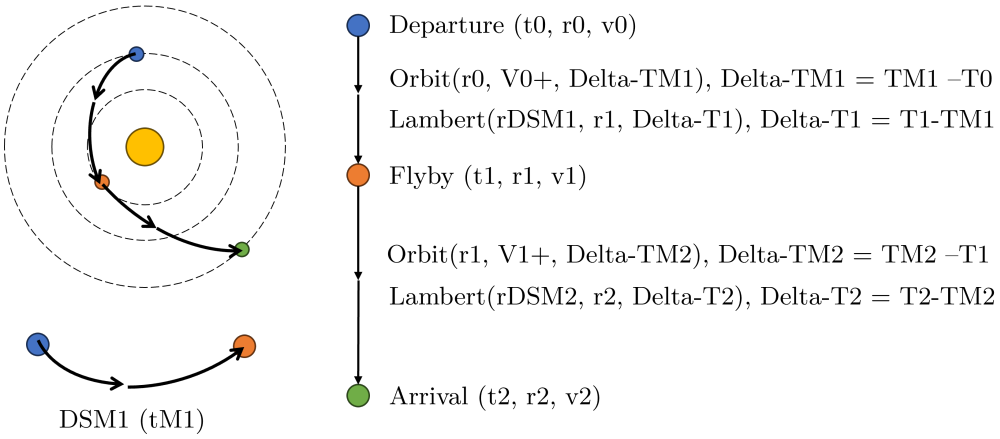

Figure 3.3: An interplanetary transfer with an intermediate flyby.

In the initial phase of each interplanetary segment, the spacecraft departs from the planet with a specific velocity and travels along a Keplerian orbit for a certain period until it reaches the point where the DSM (Deep Space Maneuver) occurs. The subsequent part of the interplanetary segment is determined by solving Lambert's problem between the point of the maneuver and the next planet, as explained earlier. At the maneuver point, a velocity discrepancy can arise, equal to the maneuver's delta-v.

Considering the above, it is possible to formulate the complete trajectory in terms of a limited number of parameters. The general case that allows a maneuver in each interplanetary segment is uniquely determined by the following variables:

- Departure instant (t_0) and 3 components for the departure velocity
- DSM instant ($t_{M,i}$)
- Flyby instant ($t_{FB,j}$) and 3 components for the velocity with which the planet is left
- Arrival instant (t_f)

A different set of variables can be used for convenience and simplicity in formulating the problem, but the minimum number of variables is expected to remain unchanged and is equal to $5N_{\text{legs}} + 1$, where N_{legs} is the number of interplanetary segments.

3.2.1 Variables

An alternative formulation in terms of variables offers several advantages:

- **Simplification of the optimization process:** As demonstrated in [7], it is possible to use an alternative set of variables to represent the velocity with which a planet is left after the flyby. Instead of using 3 Cartesian components, 3 coefficients are employed to multiply the 3 Cartesian velocity components obtained by solving the Lambert problem between one planet and the next.

$$\text{Variable Set 1} : V_{jx}, V_{jy}, V_{jz} \quad j = 1 \dots n_{FB}$$

where n_{FB} is the number of flybys.

$$\text{Variable Set 2} : L_{jx}, L_{jy}, L_{jz} \begin{cases} V_{jx} = \hat{V}_{jx} * L_{jx} \\ V_{jy} = \hat{V}_{jy} * L_{jy} \\ V_{jz} = \hat{V}_{jz} * L_{jz} \end{cases}$$

$\hat{V}$ represents the velocity obtained by solving Lambert's problem in the case where no DSMs are present. $\hat{L}_{jx}, \hat{L}_{jy}, \hat{L}_{jz}$ coefficients are multiplicative factors for velocity components and are employed as new variables.

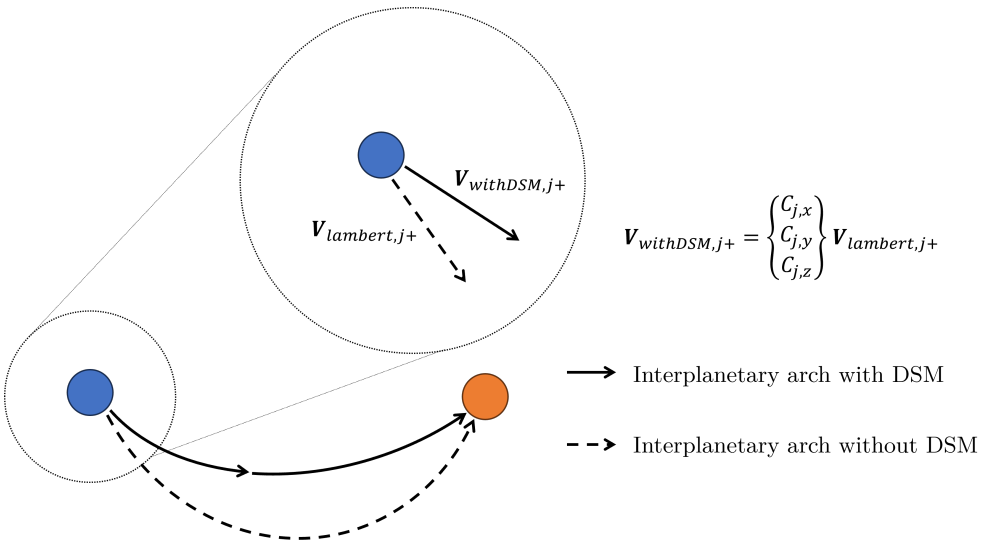

Figure 3.4: An alternative set of variables to describe the velocity with which the planet is left.

This formulation with Variable Set 2 has the advantage of being able to restrict the search space to a large neighborhood of the Lambert solution, based on the idea that generally, good solutions, even if they require DSM, do not deviate too much from the purely ballistic solution. It also offers the advantage of considering the case without DSM, where the coefficients are set to 1, as a guess solution.

- **Reduction of the number of nonlinear constraints:** It is advantageous to formulate the problem in a way that minimizes the number of nonlinear constraints whenever possible. For instance, consider the addition of a constraint on the departure asymptote declination. If a set of variables is chosen where the departure

asymptote velocity is expressed in Cartesian coordinates, it would necessitate including a nonlinear constraint on the declination angle. The presence of these constraints typically adds complexity to the optimization process. An alternative formulation in spherical coordinates allows expressing the constraint more simply as a bound for an optimization variable.

$$\text{Variable Set 1} : \begin{cases} V_{\infty x}, V_{\infty y}, V_{\infty z} \\ \text{Non-Lin. Constr. 1: } \underline{\delta} \leq \delta(\boldsymbol{V}_\infty) \leq \overline{\delta} \\ \text{Non-Lin. Constr. 2: } \underline{V_\infty} \leq V_\infty \leq \overline{V_\infty} \end{cases}$$

$$\text{Variable Set 2} : \begin{cases} V_\infty, \delta, \alpha \\ \text{Bound 1: } \underline{\delta} \leq \delta(\boldsymbol{V}_\infty) \leq \overline{\delta} \\ \text{Bound 2: } \underline{V_\infty} \leq V_\infty \leq \overline{V_\infty} \end{cases}$$

Considering the general aspects and various constraints required by this type of mission, the following set of variables has been utilized:

- **Departure:**
  - $t0$ Departure time,
  - V_∞ Magnitude of asymptotic velocity,
  - $DEC(\boldsymbol{V}_\infty)$ Declination of asymptotic velocity,
  - ΔRA Difference between the right ascension of asymptotic velocity and that of the right ascension for a transfer without intermediate maneuver (given by Lambert's problem solution).
- **Flyby:**
  - ΔT_j between the j-th flyby planet and the preceding planet,
  - $\left[\hat{L}_{jx}, \hat{L}_{jy}, \hat{L}_{jz}\right]$ Three coefficients (mentioned earlier) multiplying the respective velocity components obtained from Lambert's problem.
- **DSM (Deep Space Maneuver):**
  - η_i Coefficient expressing when during the interplanetary flight time interval the i-th DSM occurs.
- **Arrival:**
  - Δt_f between the arrival planet and the preceding one.

3.3 Model description

After modeling the trajectory as a function of a certain number of optimization variables, it is possible to formulate the cost function and constraints:

$$\begin{cases} \min J(x) = \Delta V_0 + \sum_{j=0}^{n_M} \Delta V_{Mj} + \sum_{i=0}^{n_{FB}} \Delta V_{FBi} + \Delta V_f \\ \boldsymbol{h}(x) \leq 0 \end{cases} \tag{3.2}$$

where J is the cost function and $\boldsymbol{h}$ is a vector of constraints, n_{FB} is the number of flybys and n_M is the number of deep space maneuvers. In the following sections, the contributions of the various phases are described in more detail.

Some of these phases can be modeled in different ways depending on the type of mission under consideration and the constraints to be applied.

3.3.1 Departure

For the departure phase, two different scenarios are considered (*Figure 3.5*):

- Direct Escape: The launcher takes full responsibility for providing the thrust needed to place the spacecraft on the interplanetary transfer orbit.
- Escape from Highly Elliptical Orbit (HEO): The launcher places the spacecraft on a parking orbit, typically highly elliptical. The spacecraft will then autonomously perform the escape maneuver.

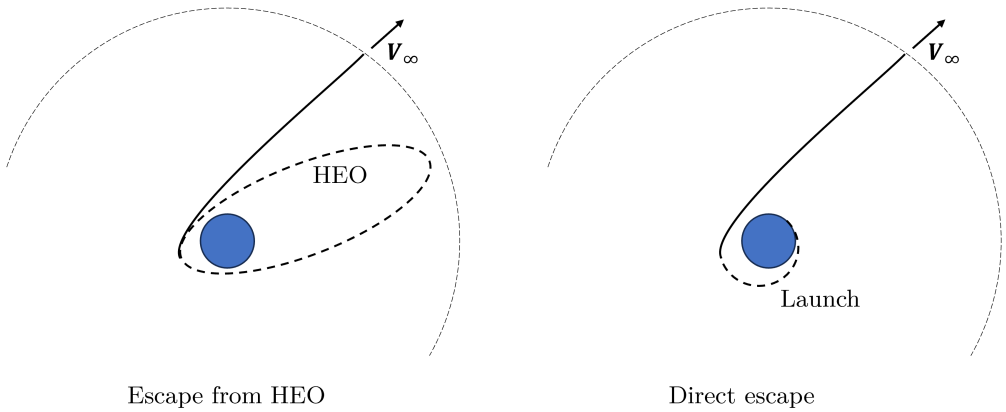

Figure 3.5: The two considered escape scenarios.

A direct escape scenario is always preferable as it avoids the need to carry additional propellant. However, the launcher's capabilities might not be sufficient to place the required mass directly in the interplanetary orbit. In such a case, the launcher puts the spacecraft on the most elliptical orbit possible, given its capabilities, to facilitate the subsequent escape.

Direct escape

In the case of a direct escape scenario, the launcher supplies the entire required delta-v, meaning that the departure does not contribute to the cost function value.

However, it is necessary to carefully consider the constraints to take into account the limitations in the launcher's capacity. The launchable mass ideally depends on the magnitude and declination of the asymptotic velocity.

The performance curves of the currently used launchers are typically not publicly shared by the launch authority. Nevertheless, data on the maximum magnitude of the asymptotic

velocity is generally available. In this case, the conservative assumption is made to limit the magnitude of the maximum declination concerning the terrestrial equatorial plane at the latitude of the launch site. With this assumption, an eastward launch is considered to maximize the launchable mass.

With a given inclination of the launch orbit (equal to the latitude of the launch site), it is possible to perform an escape with a declination magnitude equal to or less than the inclination (see e.g., [9]).

The contributions of the departure phase in a direct launch scenario to the general model are therefore as follows:

$$\begin{cases} \Delta V_0 = 0 \\ -Lat \leq \delta(\boldsymbol{V}_\infty) \leq +Lat \end{cases} \qquad Lat = \text{Latitude of the launch site}$$

Escape from HEO

As mentioned earlier, limitations in launcher performance may necessitate the spacecraft to autonomously perform the escape. The spacecraft initially resides in a parking orbit, for example, (250 km x 150,000 km), and insertion into the escape orbit occurs through a maneuver at perigee.

The use of a highly elliptical parking orbit helps reduce the required delta-v, but for typical missions, the spacecraft still needs to provide a delta-v of several hundred meters per second. Therefore, there arises the need to evaluate the delta-v of this maneuver, which constitutes the departure contribution to the objective function.

The magnitude of this impulse is usually analytically calculated based on the orbital parameters of the departure orbit and the desired asymptotic velocity.

$$\Delta V_0 = V_{des} - V_p = \sqrt{V_\infty^2 + \frac{2\mu}{r_p}} - \sqrt{(1+e)\frac{\mu}{r_p}} \tag{3.3}$$

Vdes is the desired velocity, which is the speed the spacecraft must have at perigee to enter the desired escape orbit (velocity after the maneuver). Meanwhile, Vp is the velocity at the perigee (before the maneuver). r_p and e represent the radius of the periapsis and the eccentricity of the spacecraft. μ is the gravitational parameter.

Analyzing these relationships (*Figure 3.6*, it is evident that it is advantageous to have high eccentricity and a low periastron radius to minimize the required delta-v. Furthermore, a nonlinear dependency between V_∞ and delta-v is observed.

Note that acceptable values of delta-v, below 1 km/s, given current technologies, can only be achieved with parking orbits having high eccentricities.

Gravity losses can play a significant role in this phase, given that the burn duration can extend to many minutes, rendering the assumption of impulsive burns inapplicable. In certain situations, such as when the thrusters are undersized, gravity losses become significant and must be taken into consideration even in the preliminary phase.

Since the method must apply to a preliminary analysis, gravity losses are computed separately to reduce the computational cost.

The objective is to establish relationships between V_∞ and escape delta-v that also incorporate gravity losses. To achieve this, the finite-duration maneuver was simulated

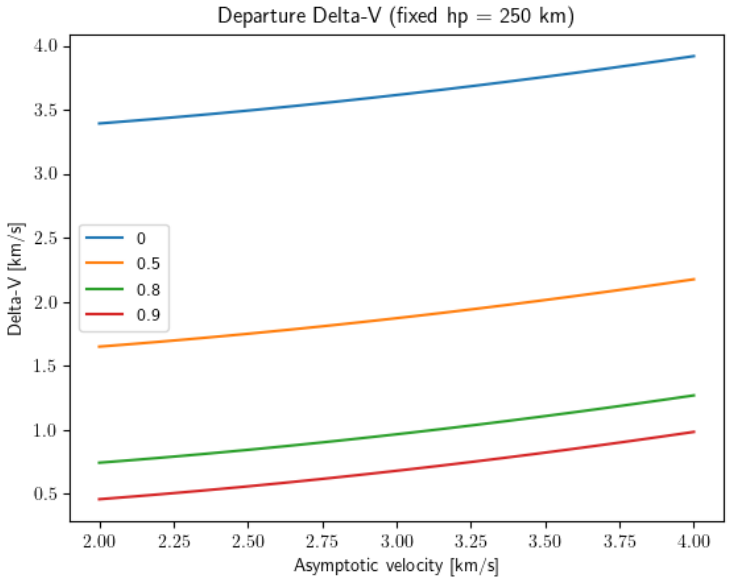

Figure 3.6: Impulsive delta-v for the escape from HEO.

separately, considering various initial mass, thrust, and specific impulse conditions to generate curves that allow obtaining the mass at the end of the maneuver and the required delta-v starting from V_∞.

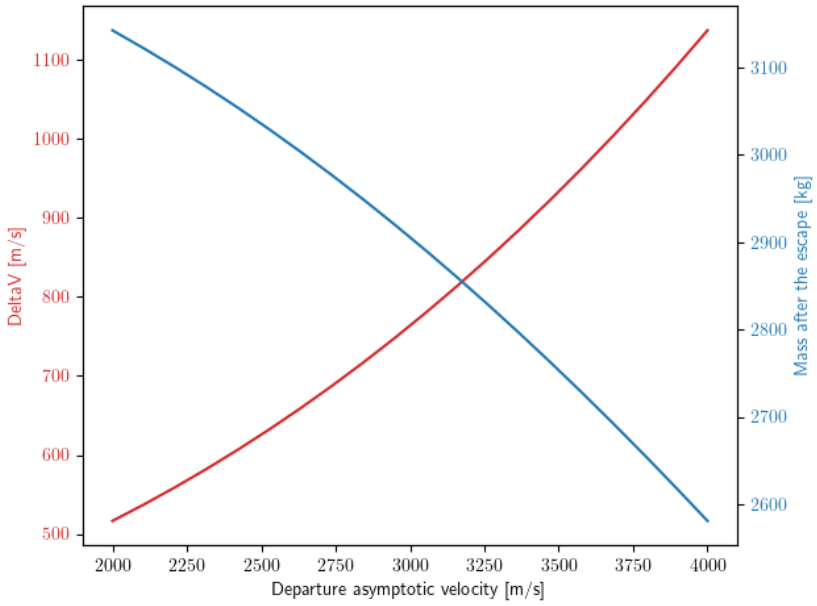

Figure 3.7: Departure Delta-V considering gravity losses.

Figure 3.7 displays the curves considered for one of the examined cases. In the case of escaping from the HEO, it is crucial to appropriately size the propulsion system of the spacecraft to minimize the burn duration as much as possible.

As in the case of direct escape, here too, a parking orbit with an inclination equal to the launch site's latitude Lat is considered. Therefore, the discussion mentioned earlier about declination holds true in this case as well.

The contribution of this phase can thus be summarized as follows:

$$\text{Ignoring GL} \begin{cases} \Delta V_0 = \sqrt{V_\infty^2 + \frac{2\mu}{r_p}} - \sqrt{(1+e)\frac{\mu}{r_p}} \\ -Lat \leq \delta(\boldsymbol{V}_\infty) \leq +Lat \end{cases}$$

$$\text{Considering GL} \begin{cases} \Delta V_0 = f(\boldsymbol{V}_\infty, T/m_0, Isp, r_{p,HEO}, e_{HEO}) \\ -Lat \leq \delta(\boldsymbol{V}_\infty) \leq +Lat \end{cases}$$

where T is the thrust, m_0 is the initial mass and Isp is the specific impulse.

3.3.2 Flyby

Flybys represent a crucial aspect of the complex interplanetary trajectories addressed in this thesis. A close encounter with a planet or moon allows for the alteration of the spacecraft's velocity without the use of propellant.

The key principle of a gravity assist is that the spacecraft's energy concerning the assisting celestial body remains constant, but its energy relative to the Sun undergoes a change. This change results from the energy exchange with the assisting planet, following Newton's laws.

In an ideal flyby, the spacecraft follows a hyperbolic trajectory with the planet located at the focus. Considering a Keplerian orbit (Figure 3.8), the asymptotic velocity maintains its magnitude because the energy is conserved in the planetocentric frame. The direction of V_∞, however, changes; consequently, when considering the heliocentric velocity, a difference is observed between before and after the flyby.

The deflection of the asymptotic velocity can be easily calculated as:

$$\cos\varphi = \frac{\boldsymbol{V}_{\infty,in} \cdot \boldsymbol{V}_{\infty,out}}{|\boldsymbol{V}_{\infty,in}||\boldsymbol{V}_{\infty,out}|} \tag{3.4}$$

In our general model, when considering a flyby, what we aim to verify is that the arrival velocity at the planet is consistent, taking into account the physics of an ideal flyby, with the velocity at which the spacecraft departs from the planet.

The minimum altitude for the flyby is set to avoid excessively close encounters, such as entering the low atmosphere. This constraint imposes an upper limit on the deflection achievable for V_∞. For a purely ballistic flyby, the following holds:

$$\sin(\delta_{max}/2) = \frac{\mu/r_p}{V_\infty^2 + \mu/r_p} \tag{3.5}$$

The minimum value of the hyperbolic excess velocity should be considered when the magnitude of the hyperbolic excess velocity before the flyby differs from the value after the flyby.

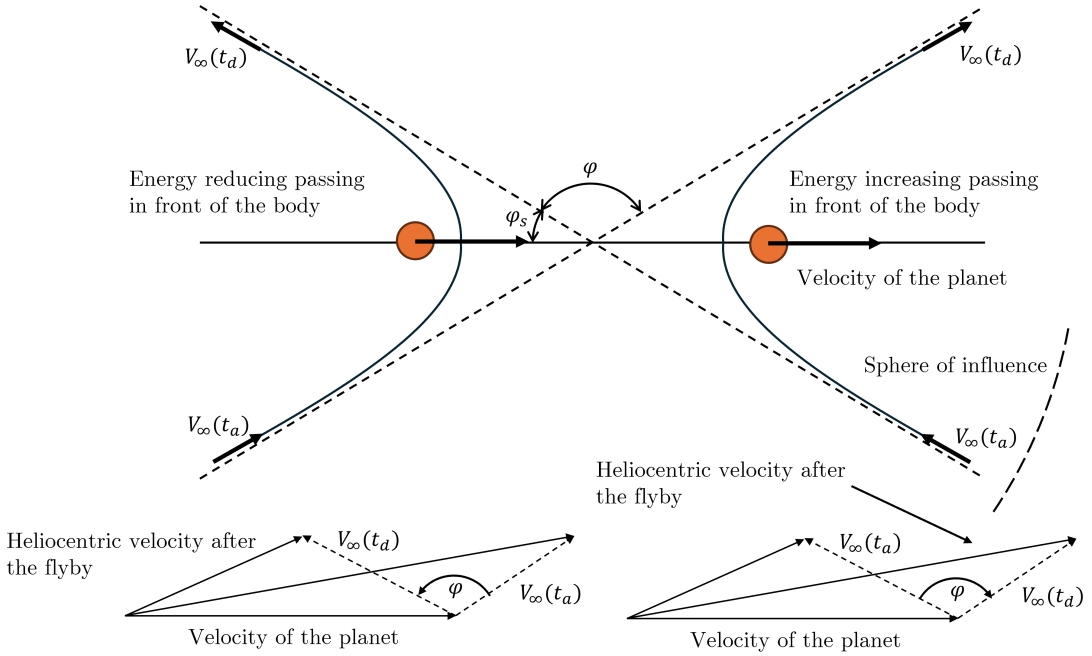

Figure 3.8: An illustration of two gravity assists: one that increases a spacecraft's energy relative to the Sun (right) and one that decreases it (left).

If the maximum rotation is not exceeded, the alteration in velocity at the flyby corresponds to the change in the magnitude of v1.

$$\Delta V_{FB,j} = |V_{\infty,out} - V_{\infty,in}| \tag{3.6}$$

Conversely, when it surpasses the maximum, the velocity rotation must be partially supplied by propulsion with an impulse either just before (when $V_{\infty,out} < V_{\infty,in}$) or after (otherwise) the flyby, as propulsion is excluded within the planet's sphere of influence.

$$\Delta V_{FB,j} = \sqrt{V_{\infty,in} + V_{\infty,out} - 2V_{\infty,in}V_{\infty,out}\cos(\delta - \delta_{max})} \tag{3.7}$$

In this scenario, the delta-v is determined using the cosine-law since the asymptotic velocity needs to be rotated to fulfill the flyby condition for maximum asymptotic velocity deflection.

3.3.3 DSM

Deep Space Maneuvers (DSMs) are maneuvers conducted in interplanetary segments, and they can contribute to minimizing the overall mission's delta-v. For instance, Cassini performed a significant DSM of approximately 450 m/s during its second flyby of Venus.

Typically, DSMs are not required in every interplanetary segment. The decision to execute a DSM or not is not determined through combinatorial variables, as that could lead to a mixed-integer optimization problem. If a DSM is deemed unnecessary in one or

more segments, its intensity will be reduced to either 0 or a very low value while evaluating the objective function

In this thesis, DSMs are obtained as discrepancies between two conditions, as illustrated in *Figure 3.9*.

The spacecraft departs from the j-th planet with a specified state expressed in the heliocentric system $\boldsymbol{r}_j$, $\boldsymbol{v}_j$ at a certain time t_j . These conditions define a Keplerian orbit. The spacecraft follows this orbit for a certain time interval indicated by the variable η_j. Thus, the conditions at the instant immediately before the maneuver $\boldsymbol{r}_{DSM,j}$, $\boldsymbol{v}_{DSM,j-}$ can be obtained.

Subsequently, the remaining interplanetary segment to the next planet is solved by addressing the Lambert problem, thereby identifying the velocity $\boldsymbol{v}_{DSM,j+}$.

The delta-v of the maneuver can be expressed as the discrepancy between the velocity immediately before and after the DSM:

$$\Delta V_{DSM,j} = |\boldsymbol{v}_{DSM,j+} - \boldsymbol{v}_{DSM,j-}|$$

In certain scenarios, it might be necessary to impose constraints on the maximum value of delta-v. This constraint could be required to lessen the overall mission complexity or for technological reasons to avoid excessively long thrust durations. In these situations, it is necessary to consider an additional constraint.

3.3.4 Arrival

The arrival phase is critical from an optimization perspective as it significantly affects the overall delta-v, and constraints on the final orbit are often the most limiting. Following the interplanetary transfer, the spacecraft must execute the insertion maneuver into the desired orbit. Since this orbit must meet various requirements, such as proper payload and communication system functioning, it is common to have several additional constraints beyond altitude and eccentricity.

One frequent requirement is related to the orbit's inclination. A polar or nearly polar orbit, for instance, is necessary to ensure global coverage for a scientific probe observing the planet.

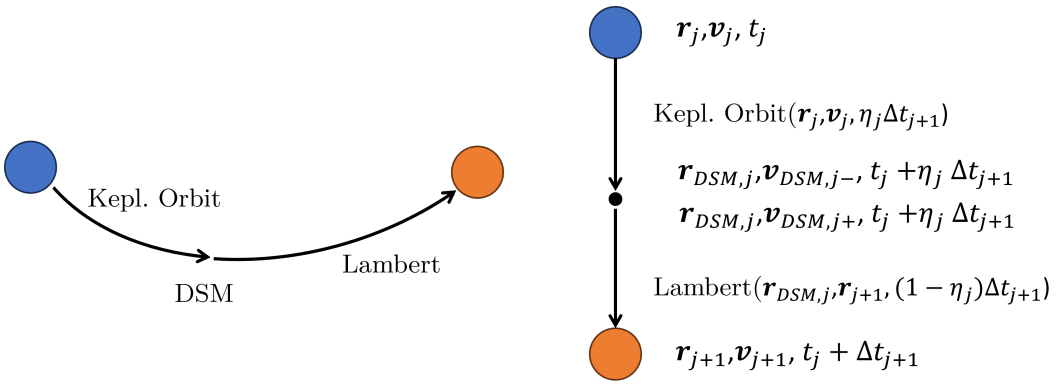

Figure 3.9: DSM Model.

Another potential requirement is the periapsis position. Constraints on the latitude of the periapsis might be necessary, especially in cases of landing or to avoid communication issues with Earth and/or eclipse duration.

For modeling this phase, two distinct cases have been considered:

1. Insertion into a target orbit: insertion into a target orbit with possible constraints on orbital parameters.
2. General rendezvous (e.g., with an asteroid): in this scenario, the spacecraft must match the heliocentric velocity of the target body.

Target orbit

The two fundamental parameters for determining the energy of insertion into a target orbit are the periapsis altitude and eccentricity. To achieve acceptable insertion delta-v values, eccentricities are usually kept high.

From a delta-v perspective, a similar approach to that used for escape has been followed. It is possible to use a basic model that involves a single impulse at periapsis.

The analytical case predicts a delta-v equal to:

$$\Delta V_f = V_{des} - V_p = \sqrt{V_\infty^2 + \frac{2\mu}{r_p}} - \sqrt{(1+e)\frac{\mu}{r_p}}$$

If gravitational losses have to be considered, the same approach of the departure phase is employed. The maneuver is simulated considering finite thrust, and tables are generated to obtain the delta-v based on the asymptotic arrival velocity and final mass. Mass must be taken into consideration because the thrust-to-mass ratio determines the duration of the burn as shown in the *Figure 3.10*.

Any inclination and periapsis latitude requirements do not directly impact the orbit's energy but impose geometric constraints on the orientation of the arrival hyperbola concerning a planetocentric reference system with the fundamental plane on the equator.

If there is a constraint on the inclination, it can be shown that there are two possible orbits for a given arrival v-infinity vector when considering a tangential impulse [10]. Furthermore, if there is also a constraint on the periapsis latitude, the orbit is uniquely determined.

Initially, it is possible to formulate the following geometric relationships among the various parameters involved in the arrival phase:

$$\begin{cases} \sin(\alpha - \Omega) = \frac{\tan\delta}{\tan i} \\ \cos(\omega + \phi) = \cos(\alpha - \Omega)\cos\delta \\ \sin(\omega + \phi) = \frac{\sin\delta}{\sin i} \\ \sin\omega \sin i = \sin LatP \\ \phi = \arccos\left[\frac{-\mu}{\mu + (R+h_p)V_\infty^2}\right] \end{cases}$$

The right ascension α and declination δ of the arrival v-infinity are known. The arrival declination restricts the possible inclinations:

$$-1 \leq \frac{\tan\delta}{\tan i} \leq 1$$

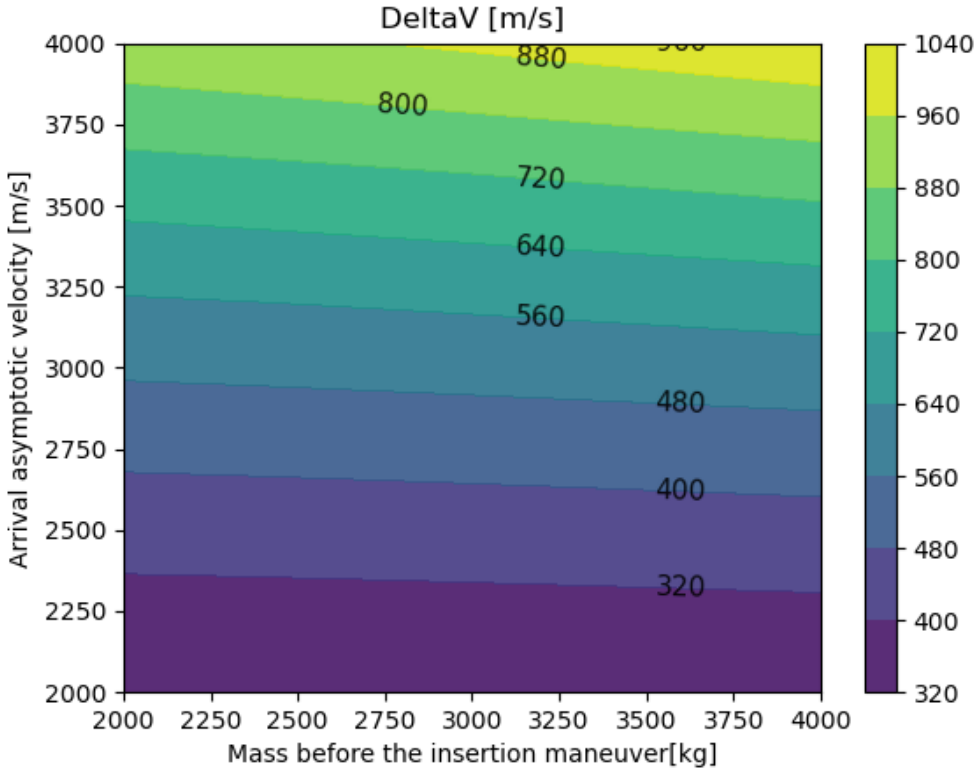

Figure 3.10: Arrival delta-v considering gravity losses.

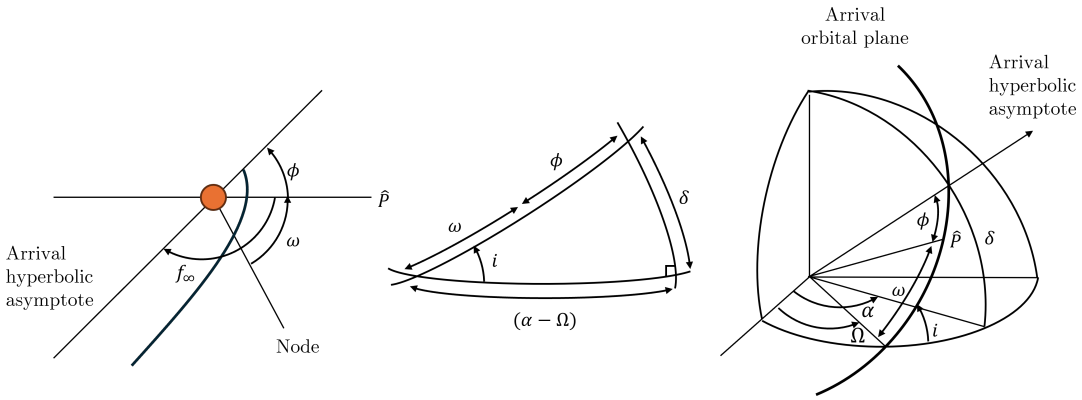

Figure 3.11: Geometry of an arrival hyperbolic orbit.

From the equations provided above, it is possible to obtain two pairs of values for the longitude of the ascending node Ω and the argument of periapsis ω. If there is a constraint on the periapsis latitude, the fourth equation comes into play, allowing the imposition of

a constraint, typically in the form of an inequality:

$$LatP \geq (LatP)_{min}$$

Rendezvous

The rendezvous case is simpler and can be used when the target is not a massive body, meaning the spacecraft does not enter orbit around it but only needs to match its velocity.

In this case, the delta-v upon arrival is simply expressed as:

$$\Delta V_f = |\boldsymbol{V}_f - \boldsymbol{V}_{target}|$$

$\boldsymbol{V}_f$ is the spacecraft's final velocity and $\boldsymbol{V}_{target}$ is the velocity of the target body.

3.3.5 Dynamics with perturbations

The simplified dynamic model seen in *Sections 3.3.1, 3.3.3, 3.3.2, 3.3.4* is valid for preliminary analyses as it allows a quick exploration of a wide range of solutions. In subsequent stages, when the mission is more defined, it is possible to consider more advanced models that take into account various sources of disturbance.

These disturbances include:

- Central Body gravity field including harmonics (CB)
- Third-body perturbation (3B)
- Solar Radiation Pressure (SRP)
- Atmospheric drag

Considering these disturbances allows obtaining the spacecraft trajectory subject to complete dynamics with the aim of achieving a continuous solution from the end of the launch phase to the arrival in the target orbit. This approach enables accurate modeling of planetocentric phases as well.

In this section, we will address the modeling of the complete dynamics, taking into account the mentioned disturbances. The formulation used is unlikely to admit a closed solution, as in the case of Keplerian orbits, and the state equation $f(\boldsymbol{r}, \boldsymbol{v}, t)$ needs to be numerically integrated.

In their most comprehensive form, considering all possible sources of perturbations, the equations take the following form:

$$f(\boldsymbol{r}, \boldsymbol{v}, t) = \begin{cases} \dot{\boldsymbol{r}} = \boldsymbol{v} \\ \dot{\boldsymbol{v}} = \boldsymbol{a} \end{cases} \qquad \boldsymbol{a} = \boldsymbol{a}_{CB} + \sum_{j=1}^{n_{3B}} a_{3Bj} + \boldsymbol{a}_{drag} + \boldsymbol{a}_{SRP} \tag{3.8}$$

where $\boldsymbol{r}, \boldsymbol{v}, \boldsymbol{a}$ respectively are position, velocity, and acceleration vectors.

Starting from these accelerations, it is possible to define the trajectory followed by the spacecraft based on initial conditions $\boldsymbol{r}_0, \boldsymbol{v}_0, t_0$. The contributions to the acceleration vector, in order, are those listed in the aforementioned list and will be discussed in the following paragraphs.

Central Body complete gravity field

To obtain the acceleration due to the complete gravitational field of a central body, it is necessary to introduce the concept of gravitational potential. The gravitational field is conservative; consequently, it is possible to associate it with a potential that, for a spherical body, takes the form:

$$U(\boldsymbol{r}) = -\frac{\mu}{r}$$

The acceleration induced by this potential is simply evaluated as:

$$a_{CB} = -\nabla U(\boldsymbol{r}) \tag{3.9}$$

For a spherical body (S), the classical point mass equation is derived as follows:

$$a_{CB} = -\nabla U_S(\boldsymbol{r}) = -\frac{\mu}{r^3}\boldsymbol{r}$$

However, the shape of the Earth, like that of other central bodies, is not spherical and is, in fact, a geoid as seen in *Figure 3.12*.

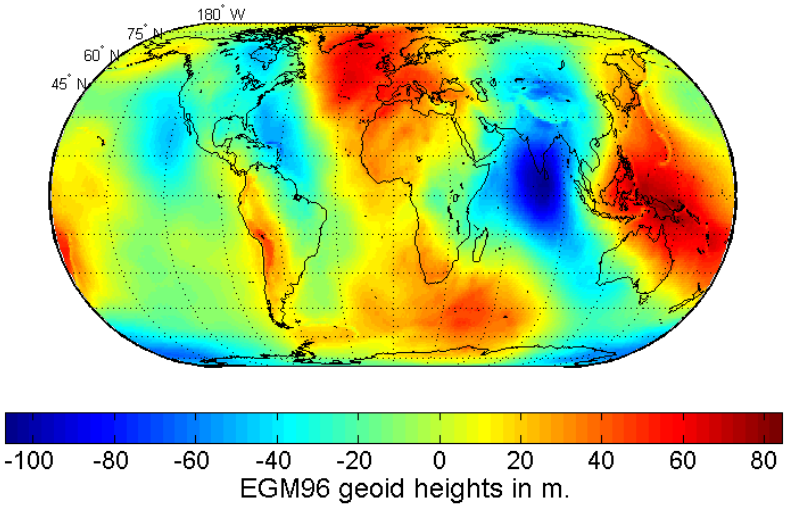

Figure 3.12: Geoid height, computed from the gravity field model EGM96 (Credits to [11]).

The geoid's shape is generally approximated through the use of spherical harmonics, based on coefficients ($C_{\ell,m}$ and $S_{\ell,m}$) obtained experimentally from measurements on past satellites:

$$U = \frac{\mu}{r}\left[1 + \sum_{\ell=2}^{\infty}\sum_{m=0}^{\ell}\left(\frac{R_{CB}}{r}\right)^{\ell} P_{\ell,m}\left[\sin(\phi)\right]\left\{C_{\ell,m}\cos(m\lambda) + S_{\ell,m}\sin(m\lambda)\right\}\right] \tag{3.10}$$

The potential is expressed in the geocentric reference system, where the position of the spacecraft is represented by r, ϕ (Latitude), and λ (Longitude). R_{CB} is the radius of the central body and $P_{\ell,m}$ denotes the Legendre polynomials.

The acceleration is then calculated as seen in *Equation 3.9* in the geocentric system. Subsequently, the vector must be transformed into the reference system in which the other quantities are expressed.

Third-body perturbation

It is possible to consider a certain number of third bodies based on the desired accuracy and the type of orbit in which a satellite is located. For example, for a Low Earth Orbit (LEO), it is already sufficient to consider the Luni-Solar disturbance, while for an interplanetary mission, several bodies are generally taken into account for different phases, with Jupiter typically predominant during interplanetary segments. The contribution of the i-th body is modeled as follows:

$$a_{3Bj} = \mu_j \left(\frac{\boldsymbol{r}_{\text{sat}j}}{r_{\text{sat}j}^3} - \frac{\boldsymbol{r}_j}{r_j^3} \right) \tag{3.11}$$

Where μ_j is the gravitational parameter of the j-th body, $\boldsymbol{r}_{\text{sat}j}$ is the position vector of the satellite relative to the j-th body, and $\boldsymbol{r}_j$ is the position vector of the j-th body relative to the central body around which the reference system is centered.

Two terms are observed: the former is called the direct effect and represents the acceleration that the third body induces on the satellite, while the latter is called indirect because it expresses the acceleration that the third body induces on the central body.

Solar Radiation Pressure

The modeling of this disturbance requires attention to two different aspects: modeling the acceleration on the spacecraft and modeling the illumination conditions on the spacecraft because solar pressure does not act during eclipses.

The expression used for the acceleration is:

$$\boldsymbol{a}_{SRP} = -p_{SRP} c_R \frac{A_{sun}}{m} \frac{\boldsymbol{r}_{sun}}{r_{sun}} \quad p_{SRP} = \frac{SF}{c} \tag{3.12}$$

where SF is the solar flux, challenging to model due to the significant variability of solar activity on both long and short time intervals. An average value is $1367\,W/m^2$. C is the speed of light. C_R is the reflectivity coefficient of the spacecraft, ranging from 0 to 2, where 0 means the object is transparent to radiation, 1 means it is a black body, and 2 means it is a perfect mirror. A_{sun} is the area of the spacecraft facing the Sun. The vector $\boldsymbol{r}_{sun}$ indicates the position of the Sun relative to the spacecraft.

As mentioned earlier, solar pressure only acts if the spacecraft is not eclipsed by a celestial body. The most frequent eclipses are those generated by the central body.

Several models define the shadow conditions on the spacecraft. Accurate models allow considering conditions of complete occultation of the solar disk (Umbra) and partial occultations (Penumbra) as in *Figure 3.13*. To assess various conditions, we first need to evaluate the apparent size of the solar disk θ_{sun} and the central body θ_{body} as seen from the satellite, along with the angular separation between the two bodies γ (See e.g., [12]).

$$\begin{cases} \theta_{sun} = \arcsin\left(\frac{R_{sun}}{r_{sun}}\right) \\ \theta_{body} = \arcsin\left(\frac{R_B}{r_{body}}\right) \\ \gamma = \arccos\left(\frac{\boldsymbol{r}_{sun} \cdot \boldsymbol{r}_{body}}{r_{sun} r_{body}}\right) \end{cases} \tag{3.13}$$

The light function takes values between 0 (total eclipse) and 1 (no eclipse) based on different cases.

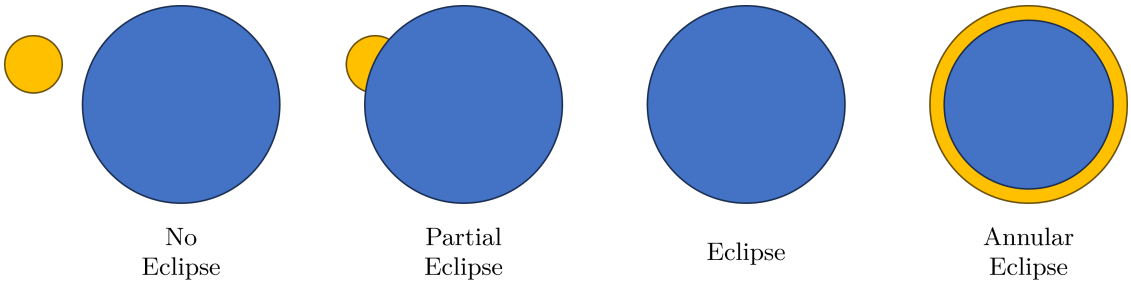

Figure 3.13: Different eclipse conditions.

$$L = \begin{cases} 1 & \text{if } \gamma - \theta_{sun} > \theta_{body} \\ 0 & \text{if } \theta_{body} > \gamma + \theta_{sun} \\ 1 - \frac{\theta_{body}^2}{\theta_{sun}^2} & \text{if } \theta_{sun} - \theta_{body} \geq \gamma \text{ or } \gamma \geq \theta_{sun} + \theta_{body} \\ 1 - \frac{A+B-C}{\pi\theta_{sun}^2} & \text{otherwise} \end{cases} \tag{3.14}$$

$$A = \theta_{body}^2 \cos^{-1}\left(\frac{\gamma^2 + \theta_{body}^2 - \theta_{sun}^2}{2\gamma\theta_{body}}\right)$$

$$B = \theta_{sun}^2 \cos^{-1}\left(\frac{\gamma^2 + \theta_{sun}^2 - \theta_{body}^2}{2\gamma\theta_{sun}}\right)$$

$$C = \frac{1}{2}\sqrt{(-\gamma + \theta_{body} + \theta_{sun})(\gamma + \theta_{body} - \theta_{sun})(\gamma + \theta_{body} + \theta_{sun})(\gamma + \theta_{body} + \theta_{sun})}$$

The obtained function L becomes a multiplicative factor for the acceleration seen in the *Equation 3.12*, thereby completing the solar radiation pressure model.

Atmospheric drag

The acceleration due to atmospheric drag is present when the spacecraft is at low altitudes and decreases rapidly with increasing altitude. The expression for this acceleration is as follows:

$$\boldsymbol{a}_{drag} = -\frac{1}{2}\frac{C_D A}{m}\rho v_r^2 \frac{\boldsymbol{v}_r}{v_r} \tag{3.15}$$

Where C_D is the drag coefficient, which is typically approximated to be around 2.2. The atmospheric density is represented by ρ, and $\boldsymbol{v}_r$ is the relative velocity with respect to the atmosphere. Atmospheric drag is arguably the most challenging perturbation source to model due to uncertainties in density and velocity values. Concerning velocity, one must consider the spacecraft's velocity relative to the atmosphere. Generally, the atmosphere is assumed to be at rest, fixed to the Earth's rotational motion. While there are models for horizontal wind, the variability in results can be high due to significant uncertainties in the models.

Density is another challenging parameter to model. Atmospheric density is not solely dependent on altitude but exhibits latitudinal and longitudinal variations. Alongside these

positional variations, there are temporal changes influenced by illumination, solar activity, variations in the Earth's magnetic field, and many other secondary effects. For these reasons, various atmospheric models have been developed over the years for different planets in the solar system. For Earth, the most used models are Jacchia-Roberts and NRLMSIS-00 (see e.g.,[13]).

Chapter 4

Experimental analysis

This chapter showcases the main results achieved. The initial section delves into specific aspects concerning the utilization of reference systems, ephemerides, and implementation. Subsequently, various analyzed cases are presented, beginning with two cases utilized for method validation, followed by an operational scenario, namely, an Earth-Venus mission. Finally, some results related to future extensions of the method are presented, where the optimization process occurs considering complete dynamics with perturbations.

4.1 Implementation

Reference Frames

Within the method, primarily two reference systems are utilized. A third reference system is added, varying according to the arrival body. For the departure phase, the terrestrial J2000 reference system is employed. It's centered on Earth's center of mass, with the X-axis pointing towards the vernal equinox at epoch J2000. The Z-axis points towards Earth's rotation axis at epoch J2000, and the Y-axis is perpendicular to X and Z axes. This system is beneficial for modeling the departure phase because its fundamental plane is the equatorial one. It's commonly used to specify orbital parameters of orbits around Earth, thus useful for defining, for example, the declination of the asymptotic departure velocity.

For the interplanetary phases, instead, the ECLIPJ2000 reference system is used, centered on the center of mass of the Sun. This is also an inertial reference system that shares the X-axis with the J2000 system but has the ecliptic plane as its fundamental plane. It is therefore rotated with respect to J2000 by an angle as shown in *Figure 4.1*. This reference system can be convenient for interplanetary phases because planets (except Mercury) and many small bodies of the solar system have orbits with small inclinations relative to the ecliptic, allowing for effective representation of interplanetary trajectories in two dimensions by considering the projection of the trajectory onto the fundamental plane.

Finally, for the arrival phase, an inertial reference system centered on the target planet is generally considered. For the case of Venus, for example, the Venus Mean Equator 2000 (VME2000) reference system is used. The reference system is centered on the center of mass of Venus and has Venus's equatorial plane as its fundamental plane. The Z-axis

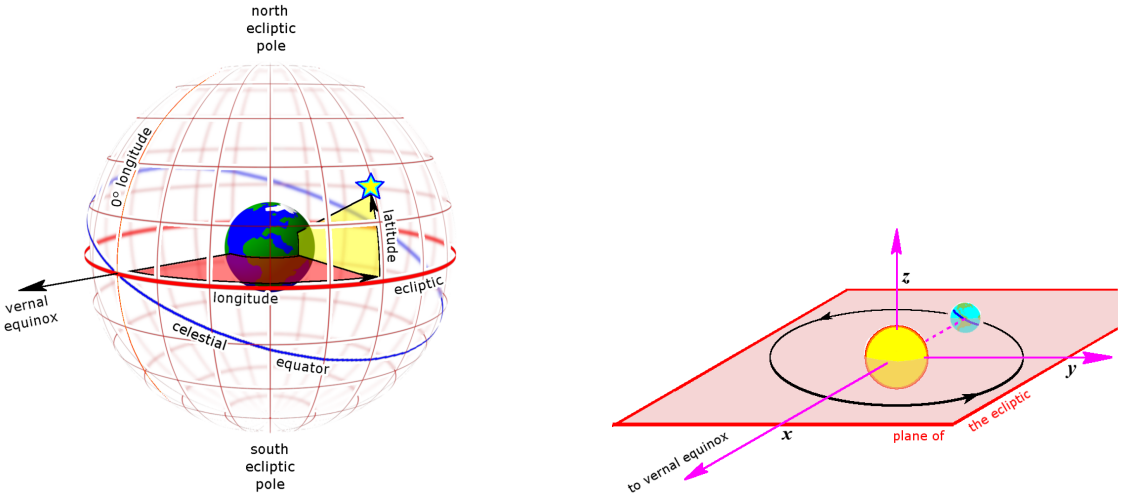

(a) Equator and celestial equator.

(b) Ecliptic reference frame.

Figure 4.1: Differences between equatorial and ecliptic reference frame.

points toward Venus North Pole of date J2000 and the X-axis points toward the Venus International Astronomical Union (IAU) vector of date J2000. The Venus IAU vector of date is defined as the intersection between the Venus equator of date and the J2000 equator, +Y axis completes the right-hand frame, In this case too, the choice of a planetocentric system with an equatorial fundamental plane is convenient because it allows obtaining the classical orbital parameters and imposing constraints on inclination and perigee latitude without further changes of the reference system.

The orientation of reference systems and rotation matrices are obtained from SPICE (Spacecraft Planet Instrument C-matrix Events), a NASA information system used to compute geometric information. SPICE was developed at NASA's Navigation and Ancillary Information Facility (NAIF), located at the Jet Propulsion Laboratory (JPL). It has become the de facto standard for handling much of the so-called observation geometry information on NASA's planetary missions and is now widely used in support of science data analysis on planetary missions of other space agencies as well.

Ephemerides

Ephemerides are widely used in this work to obtain the position and velocity of a celestial body at a given istant. The ephemerides used are the DE430, high-precision ephemerides developed by the Jet Propulsion Laboratory (JPL), also usable through the SPICE system. The planetary and lunar ephemerides DE430 are generated by fitting numerically integrated orbits of the Moon and planets to observations. The present-day lunar orbit is known to submeter accuracy through fitting lunar laser ranging data with an updated lunar gravity field from the Gravity Recovery and Interior Laboratory (GRAIL) mission. The orbits of the inner planets are known to sub-kilometer accuracy through fitting radio tracking measurements of spacecraft in orbit about them. Very long baseline interferometry measurements of spacecraft at Mars allow the orientation of the ephemeris to be tied to

the International Celestial Reference Frame with an accuracy of 0.0002 arcseconds. This orientation is the limiting error source for the orbits of the terrestrial planets and corresponds to orbit uncertainties of a few hundred meters. The orbits of Jupiter and Saturn are determined to accuracies of tens of kilometers as a result of fitting spacecraft tracking data. The orbits of Uranus, Neptune, and Pluto are determined primarily from astrometric observations, for which measurement uncertainties due to the Earth's atmosphere, combined with star catalog uncertainties, limit position accuracies to several thousand kilometers.

An alternative to using these ephemerides would be the use of simplified ephemerides, which, for example, only involve the use of Keplerian orbital parameters at a given instant and may be considered sufficient for a preliminary analysis. Since the difference in terms of computation time is minimal, it has been chosen to use the high-precision ephemerides, which also offer the advantage of also being suitable for subsequent phases of more detailed study.

Tool

The base method has been implemented in a dedicated Python tool. Python is a high-level programming language that offers the advantage of being free and open-source, and it can also be used for commercial purposes. Being a high-level language, it proves to be particularly suitable for the development of a tool that needs to be easy to use. It is widely used by the scientific community. Among Python libraries two have been provided by ESA: PyGMO [14] and Pykep [15]. The former contains various optimization algorithms, while the latter includes some functions for mission analysis, including a Lambert problem solver.

The main tool is structured into three main blocks (*Figure 4.2*): a script where the user defines one or more scenarios of interest, the main part where the black-box and optimization have been implemented, and the final part for result visualization. Additionally, a propagator that includes various disturbances has been developed in C++ for computational efficiency. This propagator is exported into a Python module for easy integration within the optimizer.

4.2 Validation of the method

The validation of mathematical models and optimization strategies plays a fundamental role. The aim of this thesis is indeed the development of a tool that can be applied with minimal user intervention to various scenarios. The tool must be capable of achieving an optimal solution, preferably global, to the given problem even in the presence of various constraints and complex profiles. Several aspects were considered in selecting the validation cases:

- Similarity of the models used.
- High number of variables.
- Presence in literature of results where the global optimum has likely been reached.

Two past interplanetary missions are considered as validation cases:

- Cassini-Huygens,

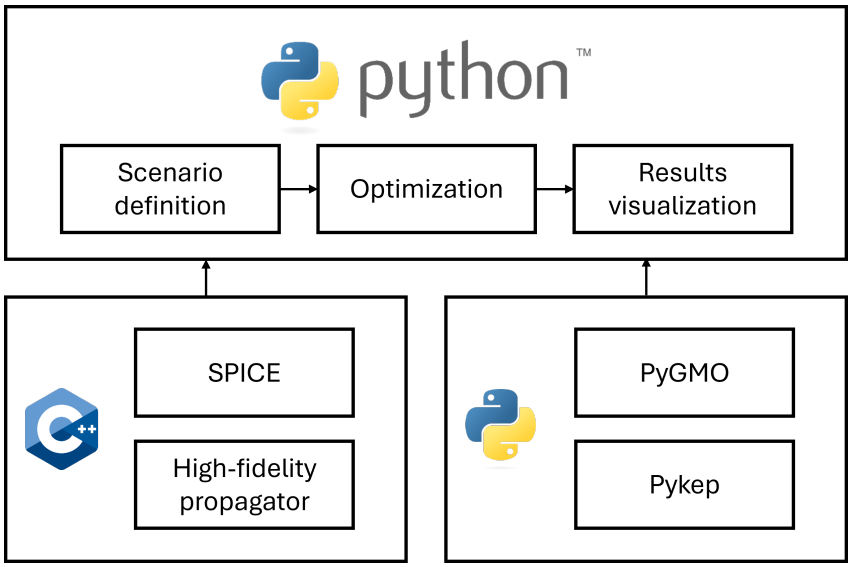

Figure 4.2: Structure of the implemented tool.

- Galileo.

4.2.1 Cassini-Huygens

The first case considered for validation is the Cassini–Huygens mission. It was an interplanetary robotic mission jointly conducted by NASA/ESA/ASI. Launched on October 15, 1997, its objective was to study the Saturn system, including its moons and rings. The probe consisted of two components: NASA's Cassini orbiter and ESA's Huygens lander. Before reaching Saturn, the probe performed flybys of Venus (in April 1998 and July 1999), Earth (August 1999), and Jupiter (December 2000). It entered Saturn's orbit on July 1, 2004. The mission ended on September 15, 2017, when the probe was deliberately sent into Saturn's upper atmosphere and destroyed to prevent any risk of contamination of Saturn's moons by potential terrestrial microorganisms on the probe.

For the validation case, the interplanetary phase of the mission, from departure to arrival at the Saturn system, was considered. Cassini serves as an ideal case for evaluation, as it presents several challenges in terms of optimization due to the numerous flybys performed.

The mission includes 4 flybys: the sequence is [Earth, Venus, Venus, Earth, Jupiter, Saturn]. The length of the sequence leads to twentysix variables for optimization using a general formulation that considers the possibility of performing a Deep Space Maneuver (DSM) in each interplanetary segment. Another difficulty arises from the presence of a resonant flyby. Resonant flybys involve passing twice over the same celestial body, as in the case of the two consecutive Venus flybys. Resonant flybys pose optimization challenges as Lambert's problem algorithms often struggle in this situation.

Cassini's trajectory includes a significant DSM of approximately 450 m/s between the two flybys, thus testing the effectiveness of the method in capturing trajectories that deviate significantly from Lambert's trajectory. Lastly, the long mission duration of approximately 7 years presents a challenge as the bounds of the temporal variables are large, resulting in a vast solution domain.

The comparison of results was made in relation to [7]. The different phases have been modeled analogously to allow for comparison. Escape is achieved through a perigee impulse of a circular reference departure orbit with an altitude of 300 km. For flybys, a minimum altitude of 300 km is considered to avoid excessive interactions with the atmosphere. Capture is accomplished through a perigee impulse, and the final orbit has an altitude equal to 0.33 x 150 Saturn radii. Considering the length of the sequence, the strategy composed by the use of the Self-Adaptive Differential Evolution (SADE) algorithm, followed by the Multistart + SQP technique, as discussed in *Chapter 2*, is employed. The interplanetary trajectory is depicted in *Figure 4.3* and *4.4*. Each encounter with a planet is represented by a black dot, while the Deep Space Maneuver (DSM) is represented by a green dot. *Table 4.1* displays the main results obtained from the trajectory optimization compared to [7].

An excellent correspondence between the two results is observed. The method proves effective in identifying the optimal times for performing the various flybys. The algorithm also succeeds in obtaining the correct Delta-V values for the DSMs, achieving the correct Delta-V for the DSM between the second and third flybys while setting the others to zero. Considering the two case studies, it can be concluded that the implemented modeling and optimization strategies are effective in achieving the optimal solution even for the analyzed complex cases. The timings of different events as well as the asymptotic velocities (Vinf) are correctly identified. In the validation cases, ideal impulsive formulations were used to evaluate the Delta-V at departure and arrival. However, since asymptotic velocities are

found correctly, it is possible to use the model accounting for gravity losses for subsequent cases.

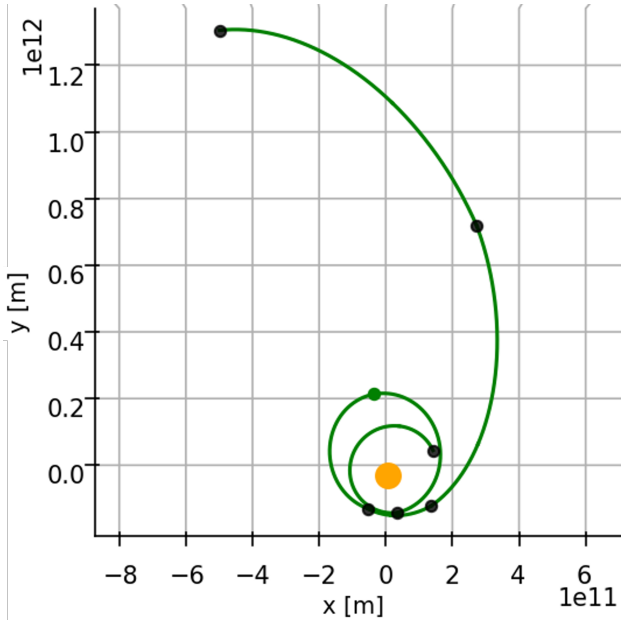

Figure 4.3: Optimized interplanetary mission profile for Cassini-Huygens in the Ecliptic J2000 reference frame.

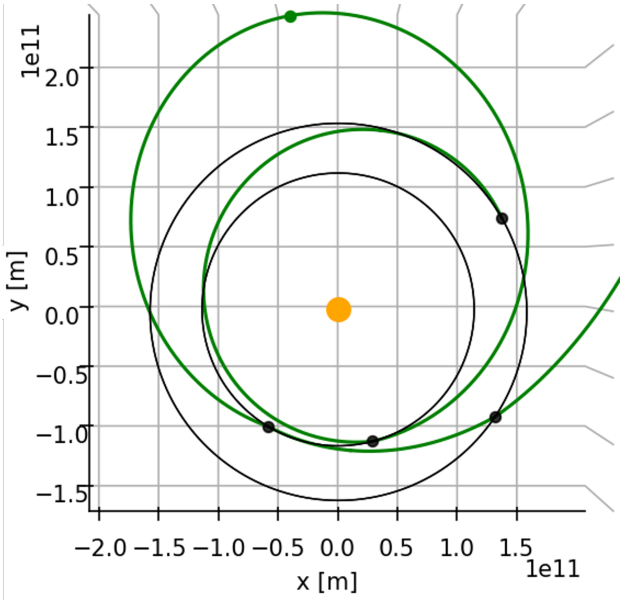

Figure 4.4: Inner solar-system phase of the optimized interplanetary mission profile for Cassini-Huygens in the Ecliptic J2000 reference frame.

		Article	**Thesis**
	Ephemerides	**DE405**	**DE432S**
Earth Departure	Date	1997-Oct-22	1997-Oct-22
	Vinf [m/s]	4009	4014
	Delta-V [m/s]	3913	3914
Venus Flyby 1	Date	1998-May-01	1998-May-01
	Vinf [m/s]	6114	6123
	rp [km]	8176	8377
DSM	Date	1998-Dec-2	1998-Dec-12
	Delta-V [m/s]	425	424
Venus Flyby 2	Date	1999-Jun-26	1999-Jun-26
	Vinf [m/s]	9295	9299
	rp [km]	6352	6421
Earth Flyby	Date	1999-Aug-18	1999-Aug-18
	Vinf [m/s]	15912	15913
	rp [km]	7437	7429
Jupiter Flyby	Date	2001-Jan-13	2001-Jan-13
	Vinf [m/s]	10218	10204
	rp [km]	9,68E+06	9,52E+06
Saturn Arrival	Date	2004-Oct-22	2004-Oct-20
	Vinf [m/s]	5102	5111
	Delta-V [m/s]	554	556
Mission	**Duration [years]**	**7**	**7**
	Delta-V [m/s]	**4892**	**4894**

Table 4.1: Results for Cassini-Huygens interplanetary trajectory.

4.2.2 Galileo

The second validation case is the Galileo mission. Galileo was a robotic space probe from the United States that conducted research on the planet Jupiter, its moons, and the asteroids Gaspra and Ida. The mission comprised an orbiter and an entry probe. It was launched into Earth orbit on October 18, 1989. Galileo reached Jupiter on December 7, 1995, following gravitational assist flybys of Venus and Earth, marking the first spacecraft to orbit an outer planet.

The sequence is [Earth, Venus, Earth, Jupiter]. Again, there is a major DSM between the two Earth flybys, and the considerations made for Cassini regarding optimization challenges apply. The interplanetary trajectory is depicted in *Figure 4.5* and *4.6*. Each encounter with a planet is depicted by a black dot, DSM is represented by a green dot.

In the referenced article [16] for Galileo, some of the data reported in the results are missing, but it is still possible to verify an excellent correspondence of the interplanetary trajectory as can be noted in *Table 4.2*.

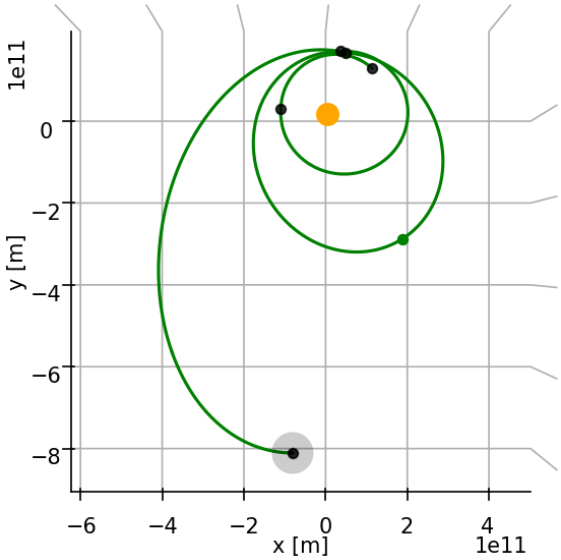

Figure 4.5: Optimized interplanetary mission profile for Galileo in the Ecliptic J2000 reference frame.

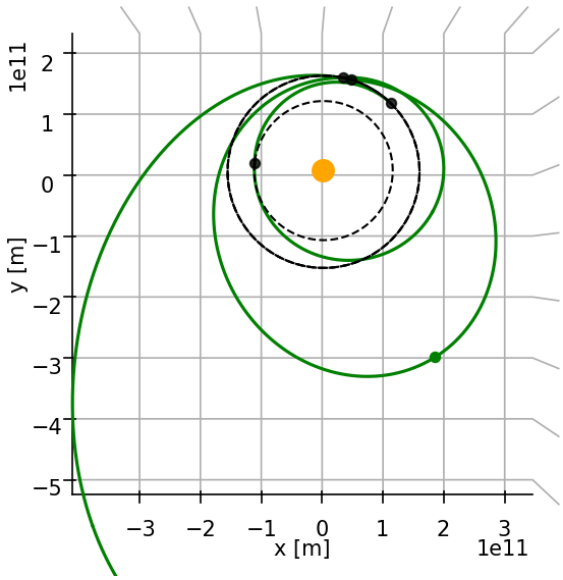

Figure 4.6: Inner solar-system phase of the optimized interplanetary mission profile for Galileo in the Ecliptic J2000 reference frame.

		Article	**Thesis**
	Ephemerides	**DE405**	**DE432S**
Earth Departure	Date	1989-Nov-06	1989-Nov-07
	Vinf [m/s]	3661	3668
	Delta-V [m/s]	3661	3668
Venus Flyby	Date	1990-Feb-20	1990-Feb-21
	Vinf [m/s]	-	4638
	rp [km]	-	19048
Earth Flyby 1	Date	1990-Dec-10	1990-Dec-10
	Vinf [m/s]	-	8349
	rp [km]	-	4038
DSM	Date	1991-Dec-22	1992-Jan-19
	Delta-V [m/s]	97	113
Earth Flyby 2	Date	1992-Dec-06	1992-Dec-04
	Vinf [m/s]	-	9004
	rp [km]	-	303
Jupiter Arrival	Date	1995-Dec-12	1995-Nov-19
	Vinf [m/s]	-	5622
	Delta-V [m/s]	809	784
Mission	**Duration [years]**	**6.1**	**6.04**
	Delta-V [m/s]	**4567**	**4565**

Table 4.2: Results for Galileo interplanetary trajectory.

4.3 Application of the method

The method has been applied to a future Earth-Venus mission within the context of ESA Envision mission. ESA Envision mission is a proposed spacecraft mission aimed at studying Venus and it is part of ESA Cosmic Vision program. Envision is designed to comprehensively investigate Venus' geology, atmosphere, and surface processes, with a particular emphasis on understanding geological history and the mechanisms driving the current environment of the planet. As reported on ESA website *Envision's fact sheet* [17]:

Envision is targeting a launch in the early 2030s. The mission is foreseen to launch from ESA's Spaceport in Kourou, French Guiana on an Ariane 62 Envision will reach Venus after a 15-month cruise. After arriving, the spacecraft will spend 15 months aerobraking through Venus' atmosphere to progressively reach its science orbit, a low Venus quasi-polar orbit, at a variable altitude of between 220 and 540 km and with an orbital period of about 94 minutes.

For the analysis, various scenarios are evaluated, taking into account the differences between performing a direct escape or an escape from a Highly Elliptical Orbit (HEO) and different flyby sequences.

Four possible sequences for the trajectory are considered:

- Earth-Venus: direct transfer case without flybys;
- Earth-Earth-Venus: intermediate flyby of Earth;
- Earth-Venus-Venus: intermediate flyby of Venus;
- Earth-Earth-Venus-Venus: longer sequence with an Earth and a Venus flyby.

The final orbit is a 250 x 250000 km elliptical orbit and is constrained both in terms of inclination and latitude of the perigee.

4.3.1 Earth-Venus trajectories

The first sequence analyzed is the direct Earth-Venus transfer without flybys. Both the case with direct escape depicted in *Figure 4.7* and the case with escape from HEO in the *Figure 4.8* are considered. The *Table 4.3* shows the main results for both cases.

		Direct Escape	**Escape from HEO**
Earth Departure	Date	2032-Dec-26	2032-Dec-27
	Vinf [m/s]	2641	2659
	Declination [°]	-2.3	-1
	Delta-V [m/s]	641	0
Venus Arrival	Date	2033-May-08	2033-May-07
	Vinf [m/s]	3736	3703
	Delta-V [m/s]	857	875
	Parking orbit	i = 88° RAAN = -165° LatP = 76°	i = 88° RAAN = 106° LatP = 74°
Mission	**Duration [days]**	**133**	**131**
	Delta-V [m/s]	**1498**	**875**

Table 4.3: Results for the Earth-Venus direct trajectories.

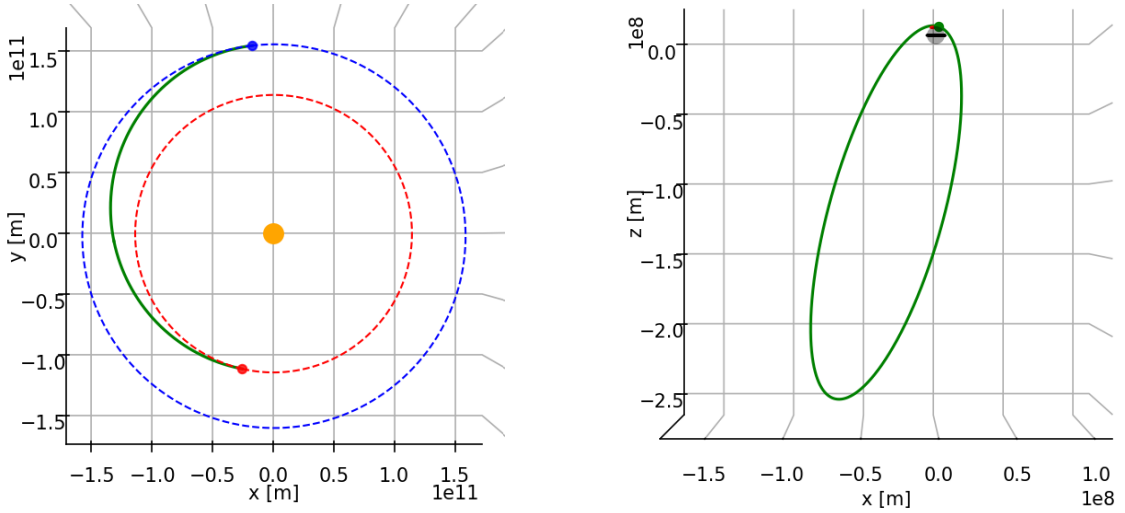

(a) Interplanetary trajectory in the ECLIPJ2000 reference frame.

(b) Orbit after the insertion in VME2000 reference frame.

Figure 4.7: Earth-Venus direct trajectory considering a direct escape.

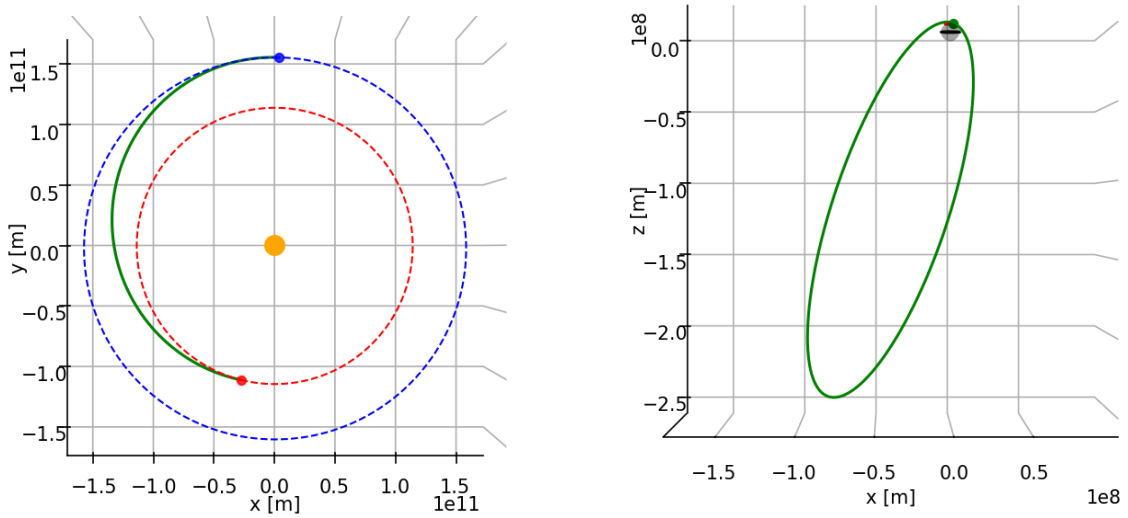

(a) Interplanetary trajectory in the ECLIPJ2000 reference frame.

(b) Orbit after the insertion in VME2000 reference frame.

Figure 4.8: Earth-Venus direct trajectory considering an escape from HEO.

4.3.2 Earth-Earth-Venus trajectories

The second sequence considered is the Earth-Earth-Venus sequence. The cases with direct escape (*Figure 4.9*) and with escape from HEO (*Figure 4.10*) for the year 2031 are considered. These two results are shown in the *Table 4.4*. In addition, the direct escape case for the year 2033 was considered (*Figure 4.11* and *Table 4.5*).

		Direct Escape	**Escape from HEO**
Earth Departure	Date	2031-Nov-28	2031-Dec-08
	Vinf [m/s]	3171	2892
	Declination [°]	-1	-4.8
	Delta-V [m/s]	0	731
Earth Flyby	Date	2032-Nov-2	2032-Dec-07
	Vinf [m/s]	3161	2911
	hp [km]	2032-Nov-27	26638
Venus Arrival	Date	2033-May-11	2033-May-07
	Vinf [m/s]	3047	3153
	Delta-V [m/s]	616	634
	Parking orbit	i = 88°	i = 88,2°
		RAAN = 175°	RAAN = -173°
		LatP = 58°	LatP = 58°
Mission	**Duration [days]**	**530**	**514**
	Delta-V [m/s]	**616**	**1365**

Table 4.4: Results for the Earth-Earth-Venus trajectories in 2031.

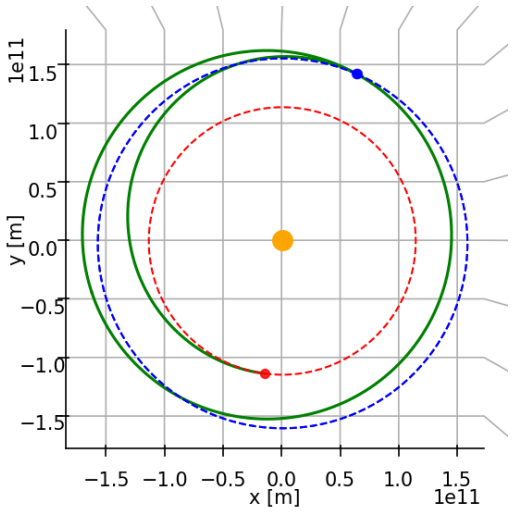

(a) Interplanetary trajectory in the ECLIPJ2000 reference frame.

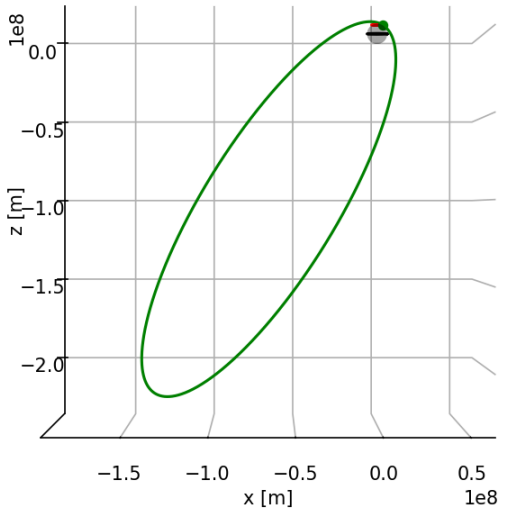

(b) Orbit after the insertion in VME2000 reference frame.

Figure 4.9: Earth-Earth-Venus trajectory in 2031 considering a direct escape.

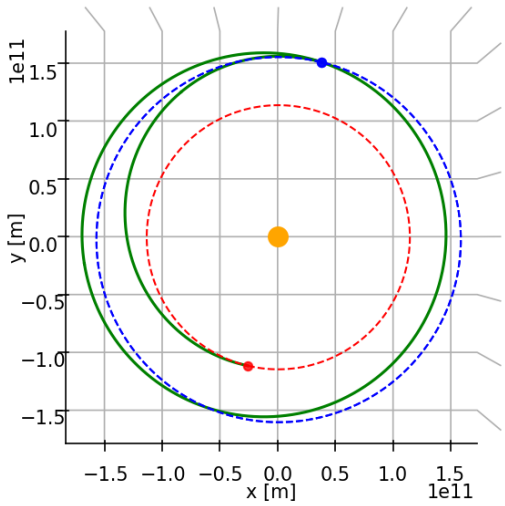

(a) Interplanetary trajectory in the ECLIPJ2000 reference frame.

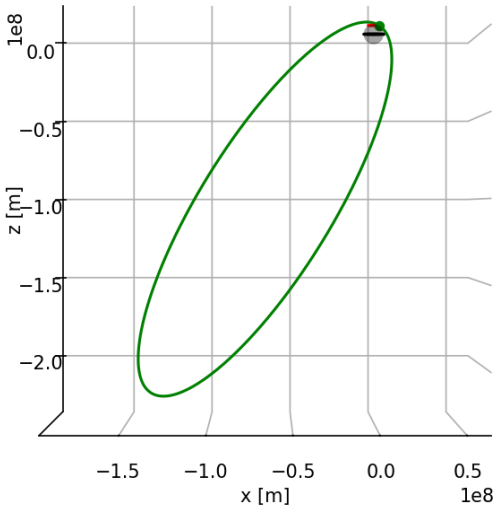

(b) Orbit after the insertion in VME2000 reference frame.

Figure 4.10: Earth-Earth-Venus trajectory in 2031 considering an escape from HEO.

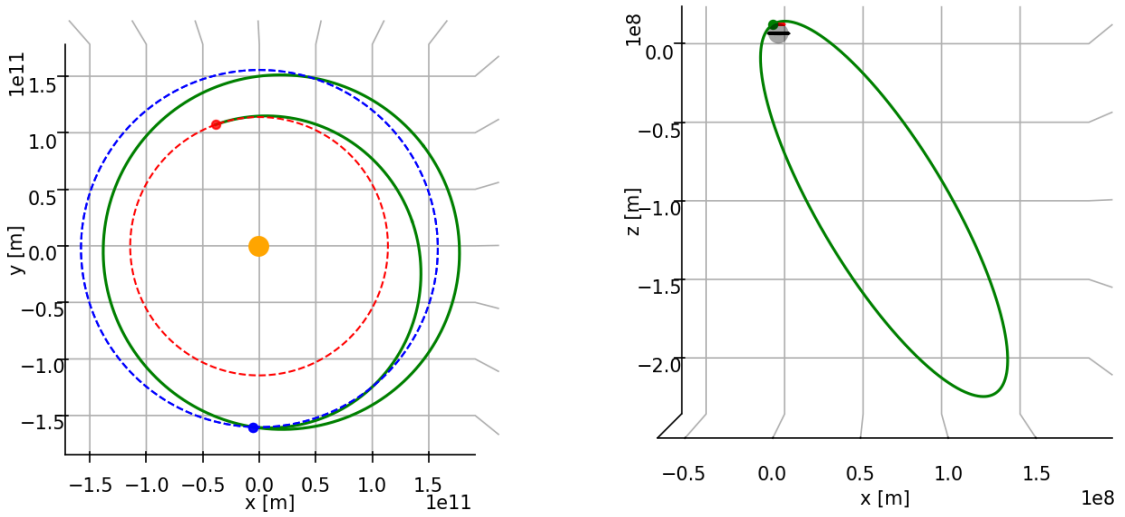

(a) Interplanetary trajectory in the ECLIPJ2000 reference frame.

(b) Orbit after the insertion in VME2000 reference frame.

Figure 4.11: Earth-Earth-Venus trajectory in 2033 considering a direct escape.

		Direct Escape
Earth Departure	Date	2033-Jun-19
	Vinf [m/s]	3944
	Declination [°]	-1
	Delta-V [m/s]	0
Earth Flyby	Date	2034-Jun-19
	Vinf [m/s]	3962
	hp [km]	10743
Venus Arrival	Date	2034-Dec-11
	Vinf [m/s]	3141
	Delta-V [m/s]	649
	Parking orbit	i = 88° RAAN = 17° LatP = 58°
Mission	**Duration [days]**	**540**
	Delta-V [m/s]	**649**

Table 4.5: Results for the Earth-Earth-Venus trajectory in 2033.

4.3.3 Earth-Venus-Venus trajectories

The third sequence considered is Earth-Venus-Venus. In this case, a launch in 2032 is considered for both the direct escape mission (*Figure 4.12*) and the HEO escape mission (*Figure 4.13*). Table *Table 4.6* shows the main results.

		Direct Escape	**Escape from HEO**
Earth Departure	Date	2032-Dec-27	2032-Dec-18
	Vinf [m/s]	2656	2657
	Declination [°]	-1	5
	DeltaV [m/s]	0	666
Earth Flyby	Date	2033-May-07	2033-May-06
	Vinf [m/s]	3703	3557
	hp [km]	887	22861
DSM	Date	2033-Jul-04	2033-Jun-25
	DeltaV [m/s]	1.8	2.5
Venus Arrival	Date	2033-Dec-18	2033-Dec-17
	Vinf [m/s]	3700	3554
	DeltaV [m/s]	874	782
	Parking orbit	i = 88°	i = 88°
		RAAN = 73°	RAAN = -104°
		LatP = 58°	LatP =58°
Mission	**Duration [days]**	**354**	**365**
	DeltaV [m/s]	**876**	**1450**

Table 4.6: Results for the Earth-Venus-Venus trajectories in 2031.

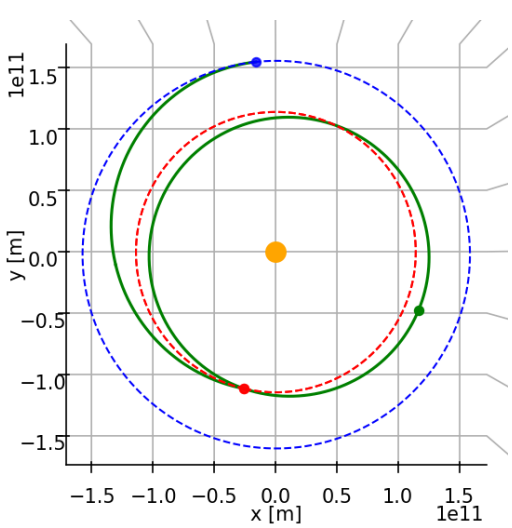

(a) Interplanetary trajectory in the ECLIPJ2000 reference frame.

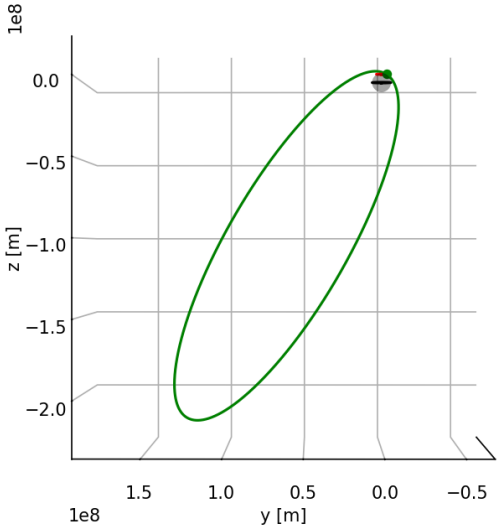

(b) Orbit after the insertion in VME2000 reference frame.

Figure 4.12: Earth-Venus-Venus trajectory in 2031 considering a direct escape.

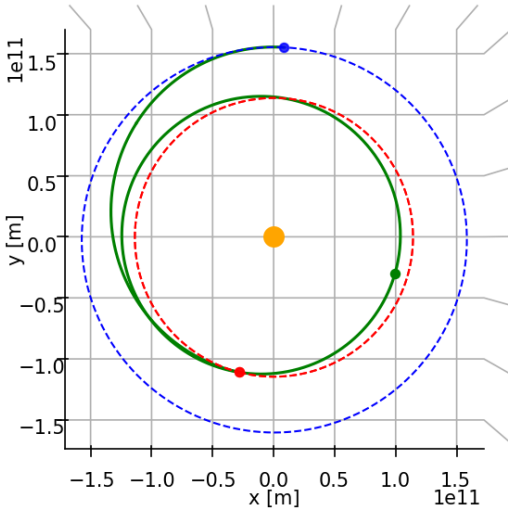

(a) Interplanetary trajectory in the ECLIPJ2000 reference frame.

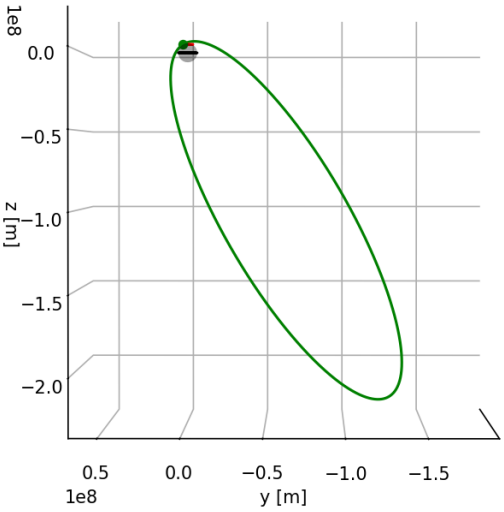

(b) Orbit after the insertion in VME2000 reference frame.

Figure 4.13: Earth-Venus-Venus trajectory considering an escape from HEO.

4.3.4 Earth-Earth-Venus-Venus trajectories

The last sequence considered is Earth-Earth-Venus-Venus. Two flybys are present in this case. Regarding direct escape, two cases are analyzed: in the first, no constraints are present on the module of the asymptotic escape velocity while in the second, an upper constraint is considered. The first case is depicted in the *Figure 4.14* and *Table 4.7*. The second is instead is reported in *Figure 4.16* and *Table 4.8*. In addition, the scenario with escape from HEO (*Figure 4.15* and *Table 4.7*) was also considered.

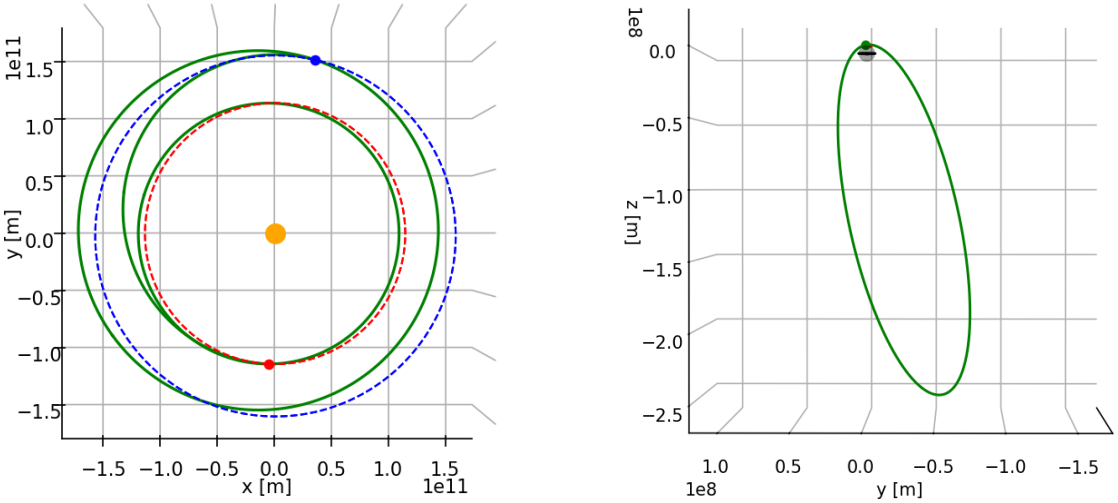

(a) Interplanetary trajectory in the ECLIPJ2000 reference frame.

(b) Orbit after the insertion in VME2000 reference frame.

Figure 4.14: Earth-Earth-Venus-Venus trajectory considering a direct escape.

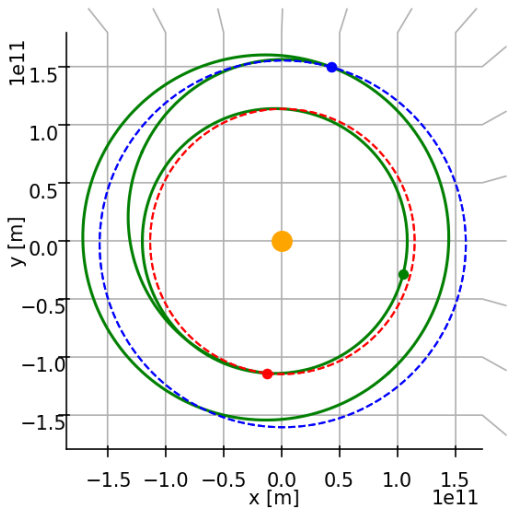

(a) Interplanetary trajectory in the ECLIPJ2000 reference frame.

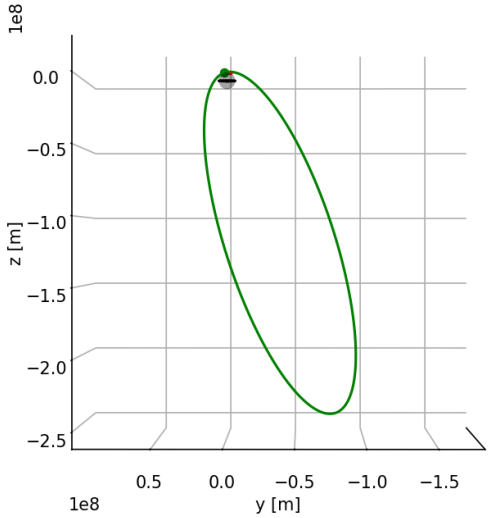

(b) Orbit after the insertion in VME2000 reference frame.

Figure 4.15: Earth-Earth-Venus-Venus trajectory considering an escape from HEO.

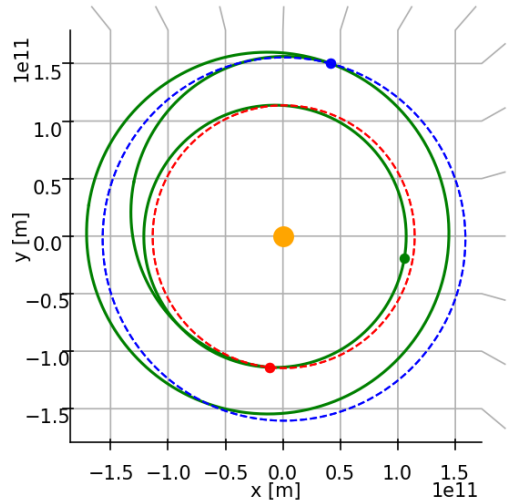

(a) Interplanetary trajectory in the ECLIPJ2000 reference frame.

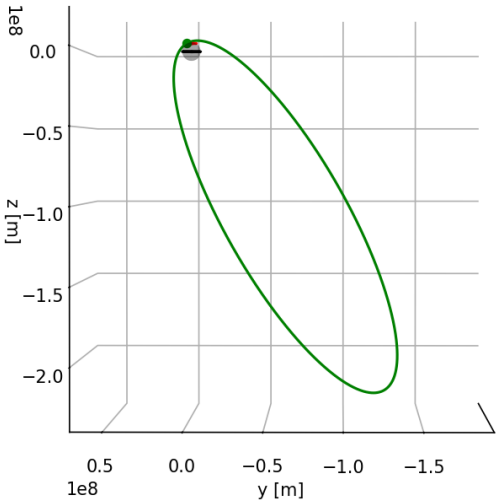

(b) Orbit after the insertion in VME2000 reference frame.

Figure 4.16: Earth-Earth-Venus-Venus trajectory considering a direct escape with a constraint on the maximum escape asymptotic velocity.

		Direct Escape	**Escape from HEO**
Earth Departure	Date	2031-Dec-09	2031-Dec-06
	Vinf [m/s]	3309	3137
	Declination [°]	-1	4.3
	Delta-V [m/s]	0	806
Earth Flyby	Date	2032-Dec-08	2032-Dec-06
	Vinf [m/s]	3330	3156
	hp [km]	12757	21781
Venus Flyby	Date	2033-May-14	2033-May-11
	Vinf [m/s]	2660	2742
	hp [km]	12510	19566
DSM	Date	-	2033-Jun-28
	Delta-V [m/s]	-	2
Venus Arrival	Date	2033-Dec-24	2033-Dec-22
	Vinf [m/s]	2660	2741
	Delta-V [m/s]	492	504
	Parking orbit	i = 88°	i = 88°
		RAAN = -93°	RAAN = -97°
		LatP =77°	LatP = 71°
Mission	**Duration [days]**	**745**	**748**
	Delta-V [m/s]	**492**	**1312**

Table 4.7: Results for the Earth-Earth-Venus-Venus trajectories.

		Direct escape with constrained asymptotic velocity
Earth Departure	Date	2031-Dec-07
	Vinf [m/s]	3160
	Declination [°]	-1
	DeltaV [m/s]	0
Earth Flyby	Date	2032-Dec-06
	Vinf [m/s]	3179
	hp [km]	18400
Venus Flyby	Date	2033-May-12
	Vinf [m/s]	2720
	hp [km]	18318
DSM	Date	2033-Jul-01
	DeltaV [m/s]	2
Venus Arrival	Date	2033-Dec-22
	Vinf [m/s]	2717
	DeltaV [m/s]	509
	Parking orbit	i = 88,2° RAAN = -96° LatP = 60°
Mission	**Duration [days]**	**748**
	DeltaV [m/s]	**511**

Table 4.8: Results for the Earth-Earth-Venus-Venus trajectory with the constraint on the maximum escape asymptotic velocity.

4.3.5 Observations

For the Envision mission, nine scenarios were considered, including four scenarios with escape from an elliptical parking orbit and five scenarios with direct escape. The method allowed for obtaining optimal solutions for all these cases while fully respecting the constraints. Herein, several graphs are presented to compare the various scenarios. In figures 4.17 and 4.18, scenarios with escape from HEO are considered. The different scenarios analyzed present different sequences of flybys. As the number of flybys increases, an improvement in terms of the overall Delta-V is observed at the expense of mission duration and complexity. In this case, there are several efficient solutions that can be considered viable. The choice of the ideal trajectory in this case must therefore be made through a trade-off that takes into account all the mission's needs. Figures 4.19 and 4.20, on the other hand, depict scenarios with direct escape. In this case, some preliminary conclusions can be drawn. The scenario with sequences EEV 2032 does not allow for a reduction in Delta-V compared to the direct transfer scenario and should therefore be excluded. In fact, in this case, increasing complexity does not bring any advantage in terms of reducing propellant mass. For the remaining scenarios, we have a similar trend to the case of escape from HEO and the choice of the trajectory must be made based on a trade-off.

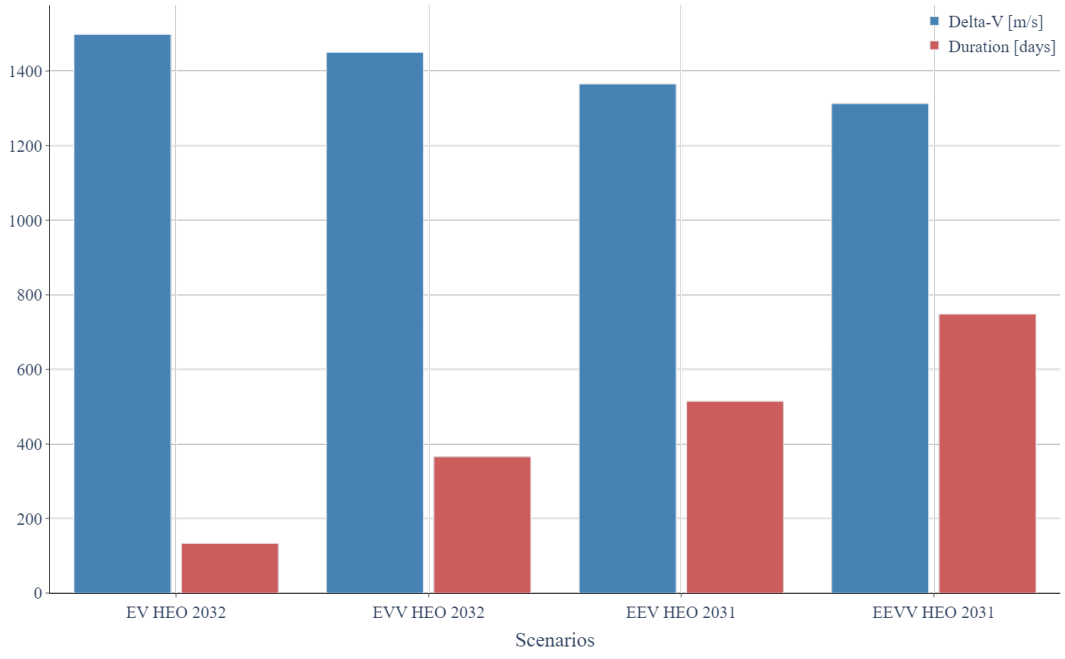

Figure 4.17: Comparison among different scenarios with departure from HEO.

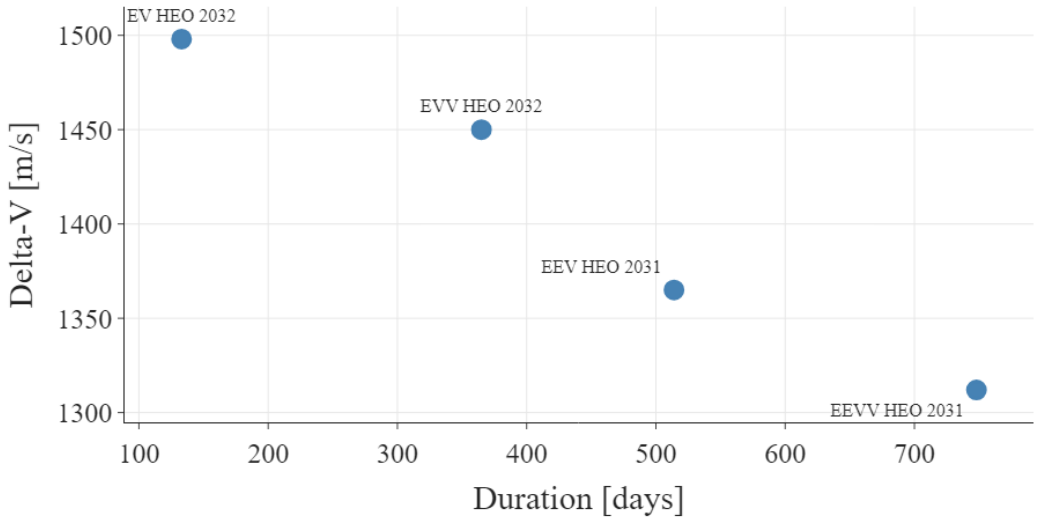

Figure 4.18: Relationship between the mission Delta-V and the duration for HEO scenarios.

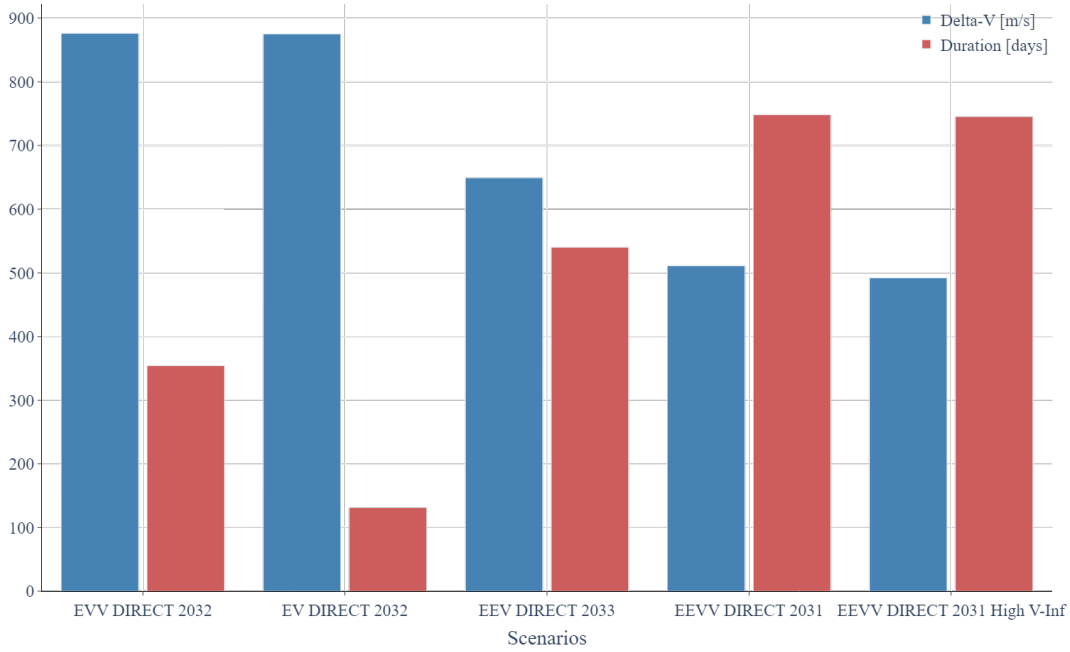

Figure 4.19: Comparison among different scenarios with direct escape.

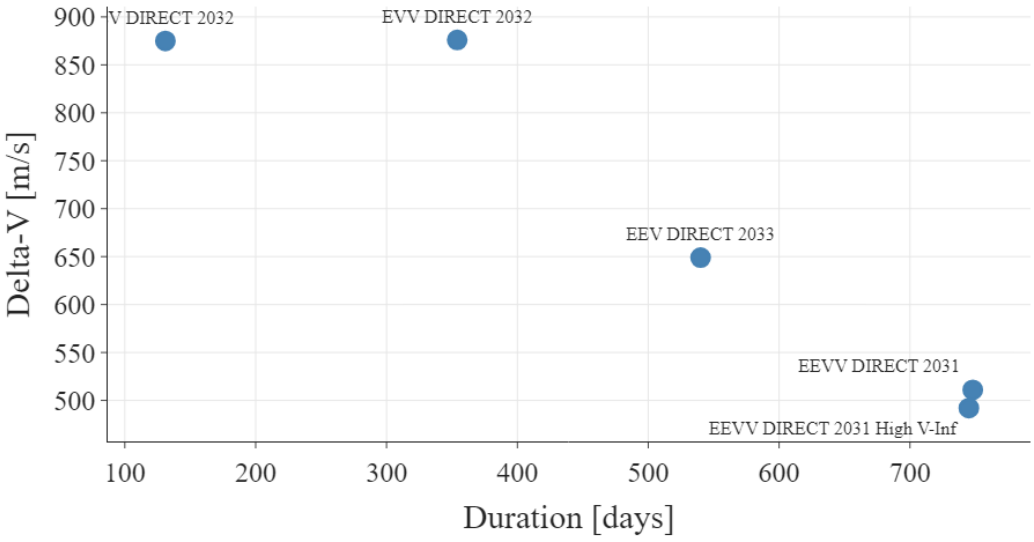

Figure 4.20: Relationship between the mission Delta-V and the duration for direct escape scenarios.

4.4 Boundary Value Problem (BVP) with complete dynamics

The method seen in *Chapters 2* and *3* has the advantage of efficiently analyzing various scenarios without starting from a trial solution, making it suitable for preliminary mission analysis studies. In more detailed phases, one of the studied profiles is typically selected. In this case, it is necessary to consider more complex dynamic models, such as those presented in *Section 3.3.5*. The final part of this work is a preliminary step towards a future extension of the method for more detailed analysis. In the method used in the thesis, solvers of the Lambert problem are extensively employed to solve the different interplanetary segments. However, these solvers can also be used in the case of Keplerian orbits. In the case of more complex dynamics where Keplerian orbits no longer apply, it is necessary to use alternative methods to solve the BVP typical of the Lambert problem. The proposed system solves a system of equations where the three components of the position vector at the end of propagation are set equal to the three components of the desired final position. The method can be defined as a shooting method where the initial velocity must be determined. The following expression holds:

$$\begin{cases} x_f(\boldsymbol{v}_0) = x_{des} \\ y_f(\boldsymbol{v}_0) = y_{des} \\ z_f(\boldsymbol{v}_0) = z_{des} \end{cases} \tag{4.1}$$

The system is solved using the Levenberg–Marquardt algorithm, starting from the velocity provided by a Lambert solver, which means starting from a tentative solution consisting

of the two-body problem solution. By solving the problem, it's possible to find an initial velocity vector $\boldsymbol{v}_0$ that is a solution to the *System 4.1*. The underlying assumption behind the use of this method is that the solution in dynamics with perturbations does not deviate excessively from that of the two-body problem. This may hold true for the cases considered, but it might not be applicable for highly perturbed orbits. In such cases, to achieve an optimal solution to the BVP, it would be necessary to adopt another strategy such as direct collocation. The method divides the considered trajectory into a certain number of sub-segments. At the endpoints of these sub-segments, the velocities necessary to reach the target position are identified. The number of points can be arbitrarily varied.

The reference trajectory is the ideal Keplerian trajectory. When considering various sources of perturbations, there is a deviation from the nominal trajectory, and the desired final position is not reached, resulting in a final position error $\Delta \boldsymbol{r}_f = \boldsymbol{r}_{des} - \boldsymbol{r}_f$. Two strategies have been adopted. The first strategy is based on bringing back the trajectory to what would be expected in the case of the two-body problem. In this case, the optimization process aims to identify the times of intermediate maneuvers. The second strategy, on the other hand, allows additional degrees of freedom in the position of these intermediate points. "Boxes" are defined to specify how much these intermediate points can deviate from the two-body solution. In this case, both the positions and times of each intermediate maneuver must be obtained solving an optimization problem. By solving the system 4.1 for each segment, it is possible to obtain the initial velocities $\boldsymbol{v}_{0,j}$ for the different segments and thus identify the Delta-Vs that must be provided at the intermediate points. The following relationship holds:

$$\Delta V_j = \boldsymbol{v}_{0,j+1} - \boldsymbol{v}_{f,j} \quad \text{with} \quad j = 1, \ldots, n_p$$

where n_p is the number of intermediate points, $j = 0$ is the departure point and $j = n_p + 1$ is the arrival point. Additionally, the velocities at the initial and final endpoints are determined.

Some cases obtained for a direct Earth-Venus transfer with departure and arrival at the edge of the sphere of influence are shown. The perturbations considered are third-body perturbations from Jupiter, Earth, and Venus and solar pressure. For all cases, the left side represents the positional error obtained by propagating the trajectory in dynamic perturbation analysis relative to the two-body solution, without altering the initial conditions and without intermediate maneuvers. On the right side, the case with corrections is represented instead. In the *Figure 4.21* the case is depicted with an intermediate point lying on the reference two-body trajectory.

The strategy proves effective in controlling the spacecraft trajectory and achieving passage through the desired points. Instead, in *Figure 4.22*, the second strategy is employed, where the maneuver point has additional degrees of freedom and does not lie on the trajectory of the two bodies. In the depicted case, a cube with a side length of 200,000 km is considered. In *Figure 4.23*, finally, the case with 2 intermediate points is depicted.

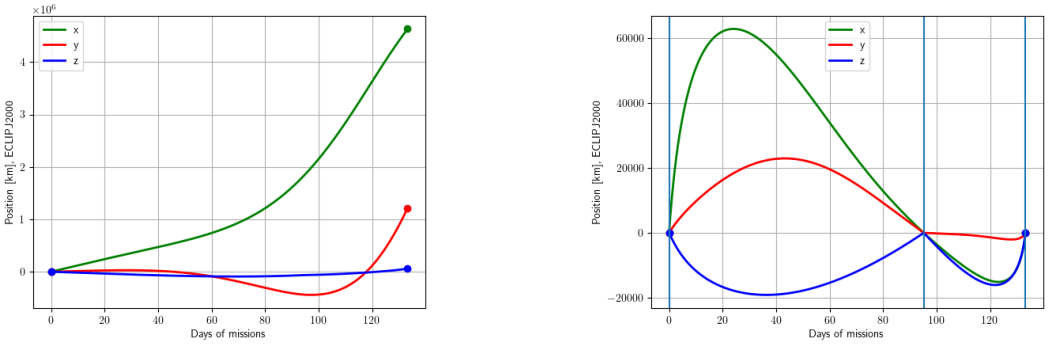

(a) Unmodified velocities. (b) Modified velocities.

Figure 4.21: Complete dynamics BVP considering one intermediate point on the two-body trajectory.

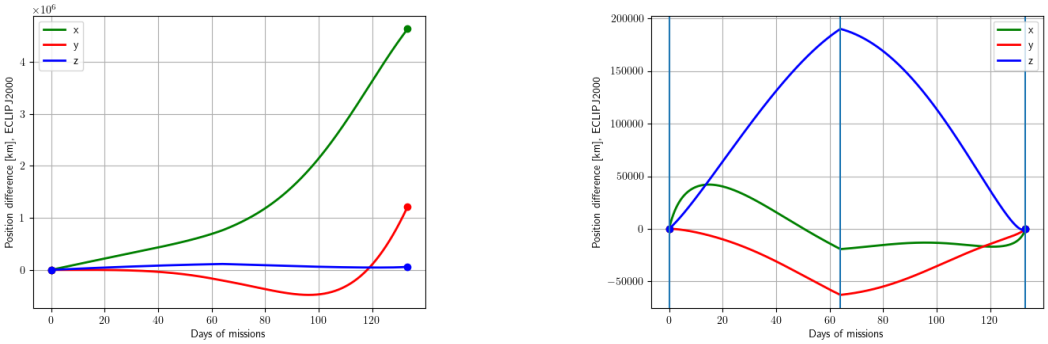

(a) Unmodified velocities. (b) Modified velocities.

Figure 4.22: Complete dynamics BVP considering one intermediate point.

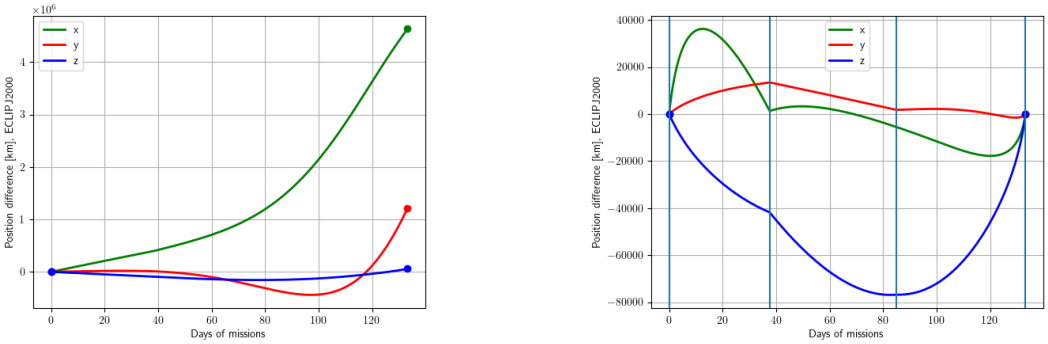

(a) Unmodified velocities. (b) Modified velocities.

Figure 4.23: Complete dynamics BVP considering two intermediate points.

Chapter 5

Conclusions and future developments

The aim of this study is to develop a method for optimizing complex interplanetary trajectories involving flybys and deep-space maneuvers. To achieve this goal, the problem is initially modeled using the simplified zero-sphere-of-influence patched conics model. This model allowed for formulating the complete problem with a limited number of variables, providing simplified dynamics while capturing its fundamental elements. A black-box optimization approach was adopted where the optimization algorithm handles the input variables of the dynamic model, based on the cost function and constraints. Due to the strong non-convexity of the problem, it was necessary to develop a global optimization strategy capable of contemplating different scenarios and reaching the optimal solution without relying on an initial guess.

Two optimization strategies were developed considering the difficulty of the problem. For cases with fewer variables, involving one or two flybys, a recursive approach using a local optimization algorithm (Sequential Quadratic Programming) from multiple starting points was employed. Following this algorithm, the solution space was further explored using an ad-hoc heuristic algorithm developed to escape local minima. A second strategy was devised to tackle more complex cases involving more than two flybys. In such instances, an initial optimization phase was added using an evolutionary algorithm, i.e, Self-Adaptive Differential Evolution, to identify satisfactory solutions. These are subsequently refined using local algorithms as described in the previous strategy.

After developing the optimization strategies, several past missions were selected to validate the method, namely the Cassini-Huygens and Galileo missions. These missions were chosen for validation due to their numerous flybys, resulting in a high number of variables, as well as their long durations requiring large bounds for variables. For both missions, extensively documented in literature, deep space maneuvers are adopted. Very good results were obtained in both validation cases, exhibiting correspondence with reference articles regarding event dates, asymptotic velocities, and DSMs. The modeling and optimization strategies proved suitable even for highly complex cases. Subsequently, the method was applied to a case of interest, a future Earth-Venus mission. Various scenarios were analyzed, involving different flyby sequences. Once again, the tool proved effective in providing

satisfactory solutions even in the presence of diverse constraints.

With the aim of expanding the method to more detailed analyses in the future, a technique was developed to solve a boundary value problem analogous to Lambert's one, where initial and final positions and times are known, and velocities at the boundaries must be determined considering a complete dynamic with perturbations. The method was implemented in a Python tool for the user input, optimization, and output display parts. The computationally intensive parts were implemented in C++. The tool is easily adaptable to different present and future scenarios, with the ability to analyze various cases and include constraints straightforwardly. In the future, the tool could be further developed to consider complete dynamics and treat the solution of the simplified model as an initial guess solution. In this regard, significant progress has already been made, but further work is needed to divide the complete mission into phases that can be properly initialized with information from the simplified solution and then optimized to obtain an ultimate trajectory solution from departure to arrival.

Bibliography

[1] *Space exploration - Milestones, Achievements, History | Britannica*. https://www.britannica.com/science/space-exploration/Major-milestones. (Accessed on 02/08/2024).

[2] A. E. Bryson and Y. C. Ho. *Applied Optimal Control*. New York: Blaisdell, 1969.

[3] M. Vasile and P. De Pascale. "Preliminary Design of Multiple Gravity-Assist Trajectories". In: *Journal of Spacecraft and Rockets* 43.4 (2006), pp. 794–805.

[4] M. Ceriotti. "Global optimisation of multiple gravity assist trajectories". PhD thesis. University of Glasgow, 2010.

[5] R. Storn and Kenneth V. Price. "Differential Evolution – A Simple and Efficient Heuristic for global Optimization over Continuous Spaces". In: *Journal of Global Optimization* 11 (1997), pp. 341–359.

[6] J. Brest et al. "Self-Adapting Control Parameters in Differential Evolution: A Comparative Study on Numerical Benchmark Problems". In: *IEEE Transactions on Evolutionary Computation* 10 (2006), pp. 646–657.

[7] M. R. Sentinella and L. Casalino. "Hybrid Evolutionary Algorithm for the Optimization of Interplanetary Trajectories". In: *Journal of Spacecraft and Rockets* 46.2 (2009), pp. 365–372.

[8] F. Glover, M. Laguna, and R. Marti. "Fundamentals of scatter search and path relinking". English. In: *Control and Cybernetics* Vol. 29, no 3 (2000), pp. 653–684.

[9] A. B. Sergeyevsky, G. C. Snyder, and R. A. Cunniff. *Interplanetary Mission Design Handbook*. Vol. 1. 2. JPL Publications, 1983.

[10] P. N. Desai and J. J. Buglia. "Determining Mars parking orbits that ensure tangential periapsis burns at arrival and departure". In: *Journal of Spacecraft and Rockets* 30.4 (1993), pp. 414–419.

[11] F. G. Lemoine et al. *Map of the undulation of the geoid in meters (based on the EGM96 gravity model and the WGS84 reference ellipsoid)*.

[12] *Circle-Circle Intersection – from Wolfram MathWorld*. https://mathworld.wolfram.com/Circle-CircleIntersection.html. (Accessed on 03/06/2024).

[13] D.A. Vallado and W.D. McClain. *Fundamentals of Astrodynamics and Applications*. Fundamentals of Astrodynamics and Applications. Microcosm Press, 2001.

[14] F. Biscani and D. Izzo. "A parallel global multiobjective framework for optimization: pagmo". In: *Journal of Open Source Software* 5.53 (2020), p. 2338. URL: https://doi.org/10.21105/joss.02338.

[15] D. Izzo. *esa/pykep: Bug fixes and more support on Equinoctial Elements*. Version v2.3. Feb. 2019.

[16] A. D. Olds, C. A. Kluever, and M. L. Cupples. "Interplanetary Mission Design Using Differential Evolution". In: *Journal of Spacecraft and Rockets* 44.5 (2007), pp. 1060–1070.

[17] *Envision's fact sheet*. https://www.esa.int/Science_Exploration/Space_Science/Envision_factsheet. (Accessed on 03/06/2024).

[18] *Ecliptic coordinate system*. https://en.wikipedia.org/wiki/Ecliptic_coordinate_system. (Accessed on 03/06/2024).